이학박사학위논문

Efficient white light generation using photonic crystal phosphors

광자결정 형광체를 이용한 효율적인 백색광 구현

2018년 2월

서울대학교 대학원

물리천문학부

이 종 호

Efficient white light generation using photonic crystal phosphors

by
Jongho Lee

Supervised by
Professor Heonsu Jeon

A Dissertation Submitted to the Faculty of

Seoul National University

in Partial Fulfillment of the Requirements

for the Degree of

Doctor of Philosophy

February 2018

Department of Physics and Astronomy
Graduate School
Seoul National University

Abstract

Efficient white light generation using photonic crystal phosphors

Jongho Lee

Majoring in Physics

Department of Physics and Astronomy

The Graduate School

Seoul National University

Generating a more efficient white light source is very important in various applications such as backlights of display panels, automobile lamps and lighting systems. In particular, white light-emitting diodes (LEDs) have gained great interest due to many unique advantages such as energy efficiency, environmental friendliness, long lifetime and compact size. The most common way to make a white light source is to combine a blue LED with one or more wavelength down-converting phosphors. In this context, phosphors are as important as blue LED chips as a component of white LEDs. Until now, however, most phosphor researches have focused on material aspects such as improvement of the performance of existing phosphor materials and development of new phosphors. As an alternative to material based approaches, our group have proposed and demonstrated a structural approach, that is, photonic crystal (PhC) phosphors. Group velocity of photon becomes zero at photonic band-edge (PBE) modes, which makes photon's interaction

with matter significantly stronger. Combining phosphors with PhC structure and tuning a PBE mode to the excitation photon energy, we obtained significantly stronger interaction between excitation photons and phosphor materials and thus much enhanced color conversion efficiency.

In this thesis, I proposed an efficient white light generation method employing a multiple stack of the structurally engineered PhC phosphors on top of a blue LED chip. I designed and fabricated the one-dimensional (1D) PhC phosphors using red and green colloidal quantum dots (CQDs), with their band-edge resonance tuned at the excitation photon wavelength. The excitation resonance improves the interaction between the excitation photons from the blue LED chip and CQDs, resulting in enhanced absorption of excitation photons by CQDs and thus enhanced emission. White light was generated by stacking the red and green PhC phosphors on a blue LED chip. I observed 8% stronger white light out of 33% less CQD amounts in comparison with the structure-less reference phosphors, thanks to a higher color conversion efficiency enabled by PBE effect.

In addition, I examined the optical properties of two-dimensional (2D) PhC phosphors. The symmetric 2D PhC phosphor exhibited enhancement factor of ~6 regardless of the polarization direction of excitation source. The asymmetric 2D PhC phosphor exhibited higher enhancement factor (~12) than other PhC phosphor structures due to the fact that both emission resonance and excitation resonance occurred.

I expect that further optimizations in structural design and device fabrication will have an enormous impact on phosphors, white LEDs and other applications requiring efficient white light.

Keyword: white light, colloidal quantum dot, photonic crystal phosphor, photonic band-edge

Student number: 2013-30118

Contents

Chapter 2

List of Tables

List of Figures

Chapter 1

Introduction

1.1 Photonic Crystals

1.1.1 Introduction

During the last decades, there have been many studies to control light, such as prohibiting propagation, confining light in specific areas, or allowing light to propagate only in certain directions. In particular, structures with periodicity have unique and novel optical properties. Photonic crystals (PhCs) are periodic arrangements of two or more dielectric materials with different refractive indices [1]. According to the direction of periodicity, PhCs are defined as one-, two-, and three-dimensional PhC structures. Figure 1-1-1 shows schematics of different types of PhCs. Scanning electron microscope (SEM) images of examples of 1D, 2D, and 3D PhCs which are realized by various fabrication methods are shown in Fig. 1-1-2; Bragg reflector, band-edge laser, and colloidal crystal, respectively [2].

The periodicity of the PhC results in a complex photonic band structure that may include photonic band-gap (PBG) and photonic band-edge (PBE). Fig. 1-1-3 is the photonic band structure of a 2D PhC. PBG is a range of frequencies where light is forbidden to propagate through PhC structure [1,3]. Due to the nature of the PBG where light propagation is forbidden, it is possible to realize various useful optical devices, for example, optical cavities [4,5] and waveguides [6,7].

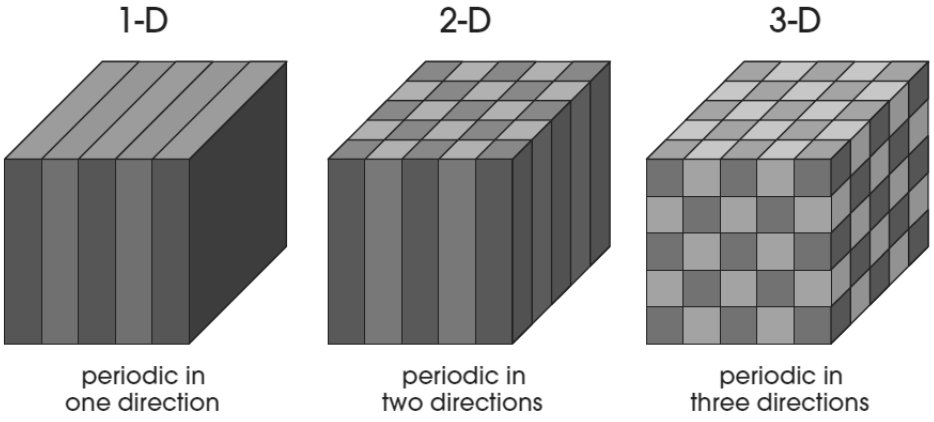

Figure 1-1-1 Schematic of representative 1D, 2D, and 3D PhCs [1].

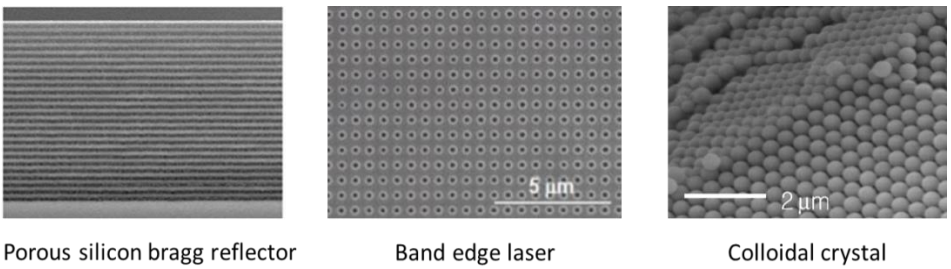

Figure 1-1-2 SEM images of examples of PhCs with sub-micron periods [2].

As an example utilizing the PBG effect, PhC cavity lasers are active devices using a high Q optical cavity surrounded by PBG. PhC waveguides are passive devices that also use PBG effects to prevent electromagnetic waves from leaking from optical path defined by the PhC region.

PBE modes also show unique and novel characteristics. At a PBE mode, the group velocity of light becomes zero, which maximizes the interaction between light and matter [8,9]. Because the PBEs are just outside the PBGs, the electromagnetic field of the PBE wavelength forms a large-area resonance mode similar to standing wave through the entire structure. As such, strong light-matter interactions in large areas can occur due to the PBE effects. PBE lasers are the most representative PBE-based devices, in which emission wavelength of photons is tuned to the PBE modes, resulting in enhanced optical gain and laser action [10,11]. As another example, the PBE modes can be used as a means to improve the absorption efficiency of photovoltaic devices such as solar cells [12-14].

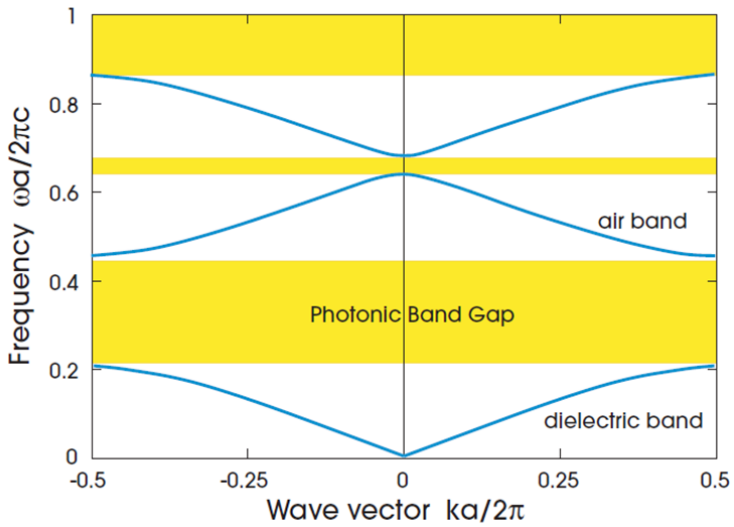

Figure 1-1-3 Photonic band structure of 1D PhC [1].

1.1.2 Photonic crystals and electronic crystals

Photons in photonic crystals having periodic permittivity and electrons in electronic crystals with periodic potential have many similarities in their characteristics. So we can explain PhCs by analogy with electronic crystals. Periodic electronic potential and distribution of periodic dielectrics, electrical energy band-gap and photonic bandgap, Schrodinger equation and Maxwell equations are the counterparts in such similarities. Table 1-1-1 shows fundamental similarities between photonics and electronics. In electronics, we can find scalar wave function $\Psi(r)$ of the distribution probability of one electron by solving the Schrodinger equation with the periodic potential $V(r)$. Contrary to the case of a free electron, the periodicity of the potential of solid crystals results in energy band-gap where electrons cannot exist. Dispersion relation between momentum and energy of one electron is shown in Figure 1-1-4(a). Similar to electronics, the propagation of light is described using a magnetic field vector $H(r)$ in photonics. At the case of periodic permittivity $\varepsilon(r)$, we can find the dispersion relationship between the frequency of wave and wave vector k by solving Maxwell equations. As shown in the Figure 1-1-4(b), the forbidden photonic band-gap where light cannot propagate exist in a certain frequency range.

Electronic Crystal	Photonic Crystal
Periodic electronic potential	Periodic dielectric distribution
Electronic band-gap	Photonic band-gap
Schrodinger equation $\left[-\frac{\hbar^2}{2m}\nabla^2 + V(\mathbf{r})\right]\psi_E(\mathbf{r}) = E\,\psi_E(\mathbf{r})$	Maxwell equation $\nabla \times \frac{1}{\varepsilon(\mathbf{r})}\nabla \times \mathbf{H}_\omega(\mathbf{r}) = \frac{\omega^2}{c^2}\mathbf{H}_\omega(\mathbf{r})$

Table 1-1-1 Comparison between electronic crystals and PhCs.

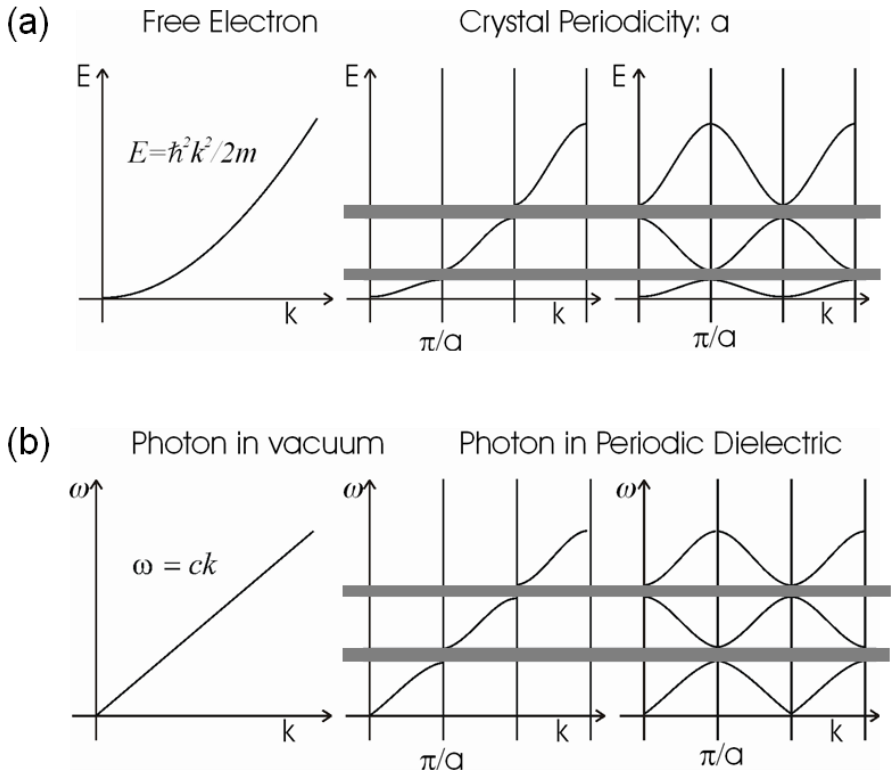

Figure 1-1-4 Dispersion relation between (a) momentum and energy of one electron in an electronic crystal, (b) frequency of electromagnetic wave and wave vector **k** in PhCs [1].

1.2 White light generation and Phosphors

1.2.1 White light generation

Light consists of three primary colors of red, green, and blue. When these three lights are combined, white light is produced. Generating a more efficient white light is very important in the applications such as backlights of display panels, automobile lamps and lighting systems. LEDs have gained great interest since the development of white light emitting diodes (LED) by Nakamura and his coworkers, due to their properties such as energy efficiency, environmental friendliness, long lifetime and compact size. The most common way to make a white light source is to combine a blue LED with one or more wavelength down-converting phosphors. Figure 1-2-1 shows various way of generating white light in solid state lighting. Among them, the most widely used is the combination of a blue LED and yellow phosphors [15].

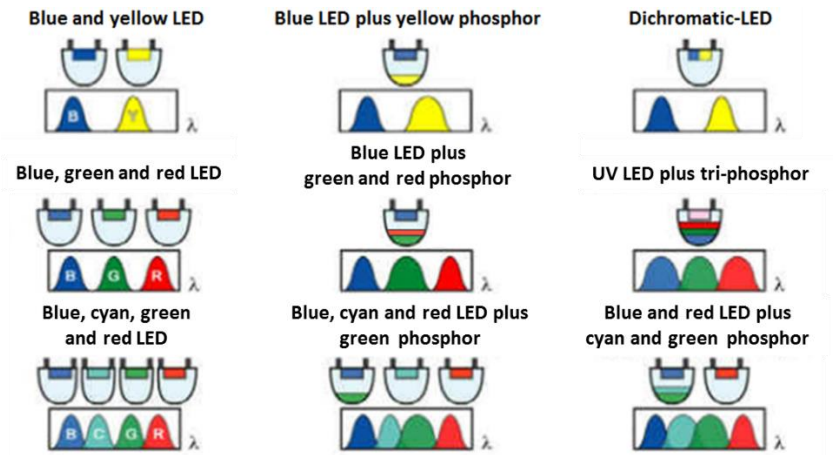

Figure 1-2-1 Various methods of generating white light in solid state lighting [15].

1.2.2 Phosphors

Phosphor is a material that absorbs excitation light and emits wavelength converted light. Figure 1-2-2 is a schematic of a white LED consisting of a blue LED chip and yellow phosphors. Some of the blue light emitted from blue LED will be converted to yellow light by the phosphors. The remaining blue light and yellow light are mixed to create white light. Figure 1-2-3 shows the spectrum of the most widely used white LED, consisting of YAG phosphors and gallium nitride (GaN) LED chip. Blue luminescence peak from GaN LED and yellow phosphorescence peak from the YAG phosphors are observed.

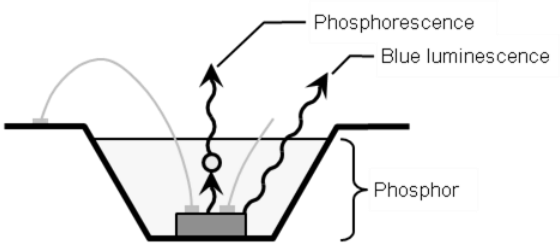

White LED (Light-emitting diode)

Figure 1-2-2 Phosphor-adopted light-emitting devices using light-emitting diodes [15].

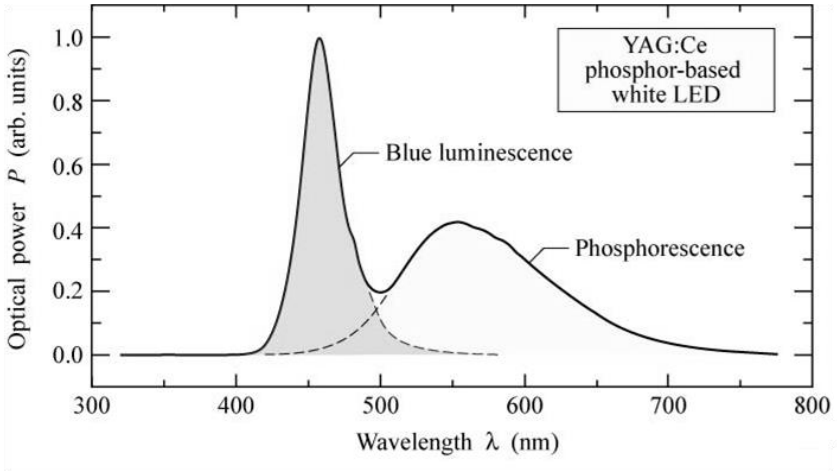

Figure 1-2-3 Emission spectrum of a phosphor-capped white LED [15].

1.2.3 Colloidal quantum dots

I used colloidal quantum dots (CQDs) because of the following advantages. First, they are suitable for our fabricated structure with submicron size patterns because of small size of individual CQD compared to other phosphors. Second, their emission wavelengths can be easily adjusted due to the quantum confinement effect of small diameters without changing the constituent semiconducting materials [16,17]. Figure 1-2-4 shows colloidal quantum dots with different diameters, exhibiting various colors. Third, the fabrication process is simple; CQDs are simply spin-coated to form a thin film. Introduction of the core-shell structure greatly improved the quantum efficiency of CQDs [18-20]. CQDs used in this study are supplied by Samsung Advanced Institute of Technology. Major procedures for CQD synthesis are provided in reference [21,22]. The red CQDs we used in the experiments have a CdSe–CdS–ZnS core–shell–shell structure whereas the green CQDs have a core–shell structure with CdSeS alloyed core and ZnS shell. Figure 1-2-5 (a) and (b) show TEM images of the red and green CQDs, respectively, from which physical dimensions of the CQDs are analyzed. The histograms on the CQD size distributions are shown in Figure 1-2-6 (a) and (b); the average sizes of the red and green CQDs are 8.05 ± 0.87 nm and 7.16 ± 0.76 nm, respectively. The complex refractive indices of red and green CQD films obtained from spectroscopic ellipsometry measurements were shown in Figure 1-2-7 (a) and (b), respectively. Figure 1-2-8 show emission spectra of the red and green CQDs, respectively; the center emission wavelengths of the red and green CQDs are 610nm and 530nm, respectively.

Figure 1-2-4 Colloidal quantum dots with different diameters, exhibiting various colors [23].

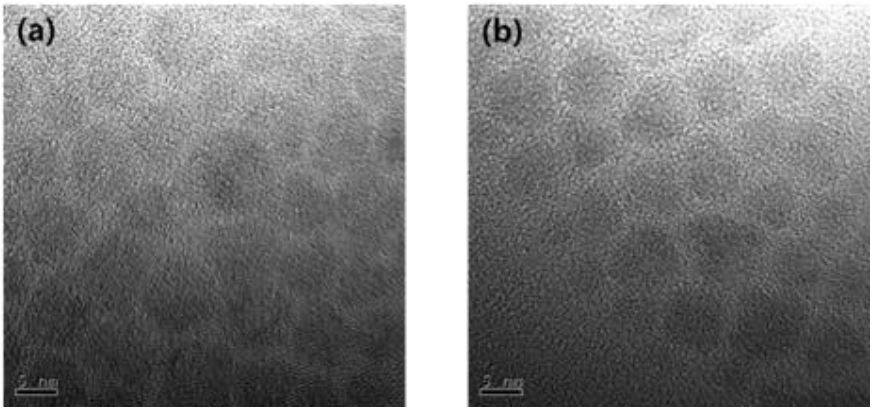

Figure 1-2-5 TEM images of red (a) and green (b) CQDs.

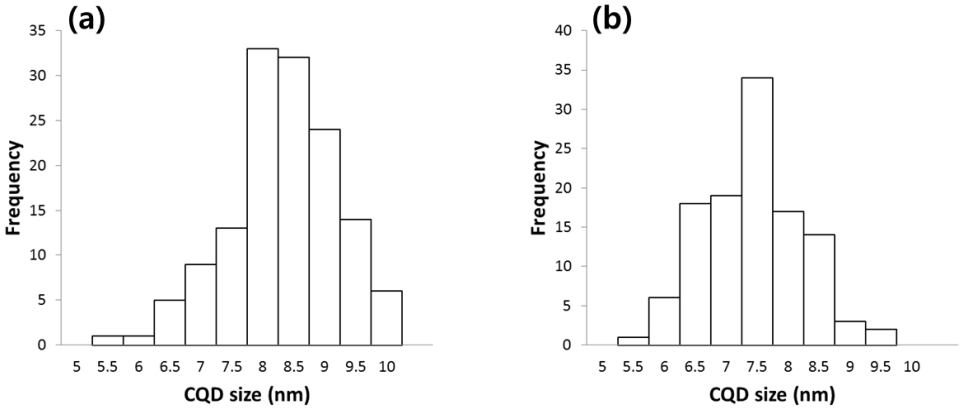

Figure 1-2-6 Histograms on size distributions of red (a) and green (b) CQDs.

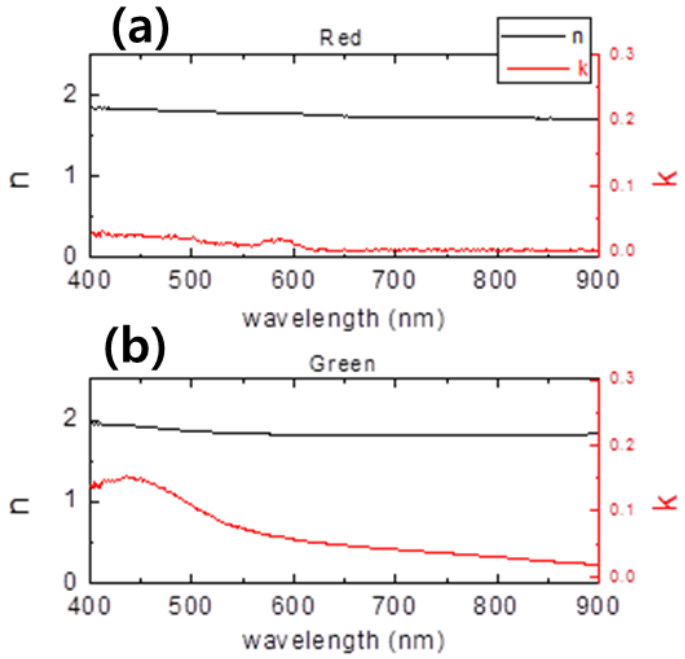

Figure 1-2-7 Complex refractive indices of red (a) and green (b) CQDs.

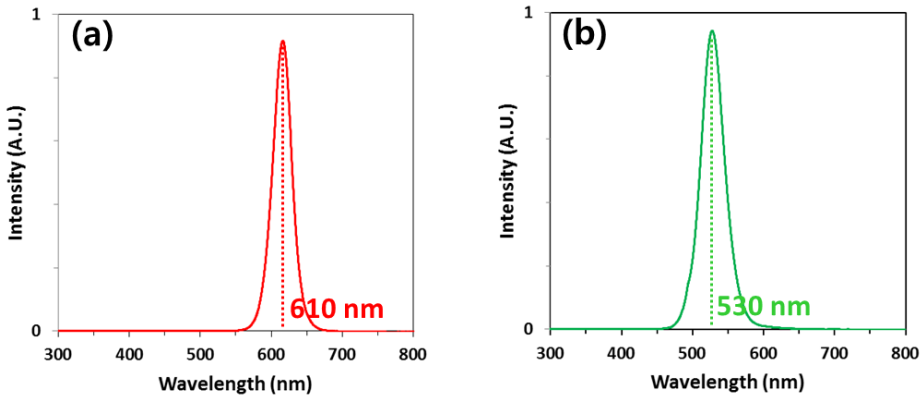

Figure 1-2-8 Emission spectra of red (a) and green (b) CQDs.

1.3 Photonic crystal phosphors

The external quantum efficiency (EQE) η_{external} (or color conversion efficiency) is given by

$$\eta_{\mathrm{external}} = (\text{Absorbance of pump photons by phosphors}) \times \eta_{\mathrm{internal}} .$$

the internal quantum efficiency (IQE) η_{internal} is defined as the ratio of number of photons emitted from the phosphor molecules by number of pump photons absorbed by phosphors.

Until now, most phosphor researches have focused on materials development, for example, to achieve a higher color-conversion efficiency or to adjust the absorption/emission bands to desired spectral ranges [24-27]. Although much progress has been made, phosphor developments through such conventional material-oriented approaches will be limited or saturated eventually. As a paradigm shift in phosphor developments, the authors' group have proposed and demonstrated a structural approach, that is, photonic crystal (PhC) phosphors [28-30].

By carving phosphor materials into a PhC structure and subsequently tuning the excitation photon energy to a photonic band-edge (PBE) mode, where the photon group velocity becomes zero [8,9], we can relish a significantly strengthened interaction between excitation photons and phosphor materials and thus an improved color conversion efficiency (regardless of phosphor materials employed) [28-30].

Figure 1-3-2 shows preceding researches conducted in our group. The color conversion efficiency of the vertical one-dimensional (1D) PhC phosphor was

increased by 1.36 times as compared with that of the reference phosphor (left), and lateral 1D PhC phosphor showed 4-fold enhancement of fluorescence intensity over the reference phosphor (right).

In this thesis, I proposed an efficient white light generation method employing a multiple stack of the structurally engineered PhC phosphors on top of a blue LED chip. I investigated the performance characteristics of a lateral 1D PhC phosphor, a 1D grating structure composed of alternately arrange colloidal quantum dots (CQDs) and Si_3N_4. Based on these results, red and green PhC phosphors optimized for blue LED were designed and fabricated. Finally, the prepared photonic crystal phosphors are stacked on top of a blue LED to generate efficient white light.

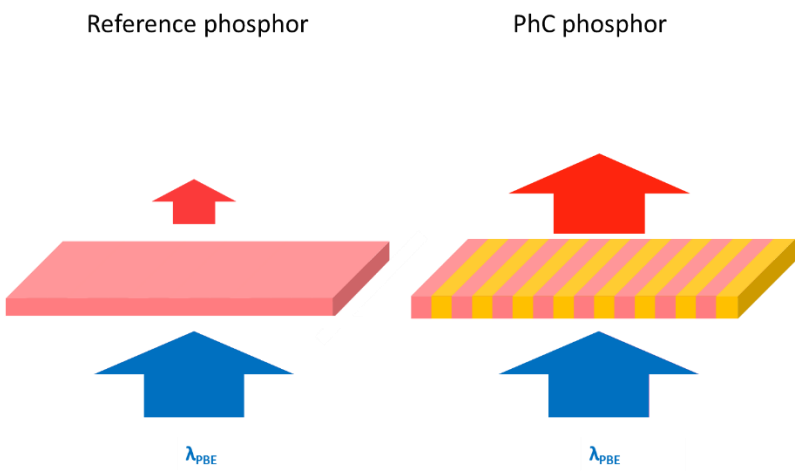

Figure 1-3-1 Comparison between PhC phosphor and reference phosphor.

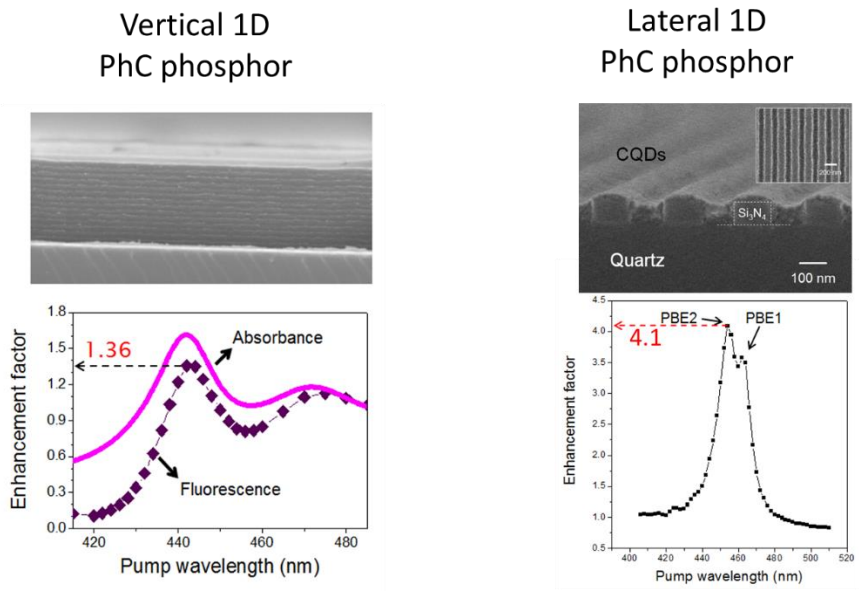

Figure 1-3-2 Two types of 1D PhC phosphors characterized by directions of periodicity: vertical 1D PhC phosphor (left) and lateral 1D PhC phosphor (right).

1.4 Computational Method

1.4.1 Plane-wave expansion method

Plane-wave expansion (PWE) method is a computational algorithm to solve Maxwell's equations in infinitely periodic media. It is very useful and powerful technique for investigation of the photonic band structure of any types of PhCs. Especially, in 2D simulations, the PWE method quickly gets modal solutions that describe the photonic band and field profile. To solve Maxwell's equations using PWE, electric fields and magnetic fields are expanded in terms of Fourier components along their reciprocal lattice vector. Sets of differential equations are formulated to an infinite matrix eigenvalue problem, which can be solved after proper approximation [31,32].

I used BandSOLVE (Rsoft Design Group), commercial software based on PWE, to investigate the photonic band structure of PhC phosphors in Chapter 2 and 3.

1.4.2 Finite-difference time-domain method

Finite-difference time-domain (FDTD) method is a widely used numerical analysis method dividing space into discrete, mesh-like grids in which each of the electric fields and magnetic fields are analyzed in discrete time steps. Unlike PWE method with approximations in processes or limitations in boundary conditions, most solutions of the time dependent Maxwell's equations can be solved exactly with no approximation in processes, and with no limitation in boundary conditions. The accuracy of solutions and computation time depends on the size of the grids and time steps [33].

Commercially available software, Lumerical FDTD Solutions (Lumerical Solutions, Inc.) was used to calculate the photonic band structures, electric field profiles of the PBE modes, and absorbance of the PhC phosphors in Chapter 2 and 3.

1.4.3 Transfer-matrix method

The transfer-matrix (TM) method is an effective way of describing light propagation through various media within the scope of ray optics. From Maxwell's equations we can get two matrices about the behavior of the photons propagating in homogeneous medium and crossing the boundary between different media. Based on the two kinds of matrices, one can finally solve the wave equation of electromagnetic waves passing through various media. This process is quite simple enough to be solved analytically by hand [34]. Furthermore, wave equations can be solved accurately by applying analytic solutions to computer software products such as Mathcad, MATLAB, and Mathematica.

I calculated the confinement factor Γ and the effective refractive index n_{eff} in the 2D PhC phosphor structure using the TM method in Chapter 3.

1.5 Outline of the Manuscript

I proposed an efficient white light source platform using structurally engineered PhC phosphors. I investigated the characteristics of PhC phosphors. The photonic crystal phosphors were stacked on top of a blue LED to generate efficient white light.

In chapter 2, I proposed an efficient white light generatoin method using CQD based PhC phosphors. I investigated the optical properties of a lateral 1D PhC phosphor, a 1D grating structure composed of alternately arrange colloidal quantum dots (CQDs) and Si_3N_4. Based on these results, the red and green PhC phosphors, their photonic band-edge modes were matched to the excitation photon energy, were designed and fabricated. The prepared PhC phosphors were stacked on top of a blue LED chip to generate efficient white light.

In chapter 3, I investigated the performance characteristics of 2D PhC phosphors. I calculated the photonics band structure and absorbance spectra of symmetric and asymmetric 2D PhC phosphors by computational method such as FWE and FDTD. The symmetric and asymmetric 2D PhC phosphors were designed and fabricated, and the characteristics such as PL enhancement factor at the PBE wavelength and dependence on excitation source polarization were explored.

Finally, in chapter 4, the conclusion is presented.

References

[1] John D. Joannopoulos, Robert D. Meade, and Joshua N. Winn, *Photonic crystals: Molding the flow of light* (Princeton University Press 2008).

[2] http://mnoel.snu.ac.kr/

[3] E. Yablonovitch, "Inhibited spontaneous emission in solid-state physics and electronics," Phys. Rev. Lett. **58**, 2059-2062 (1987).

[4] H. Yokoyama, "Physics and device applications of optical microcavities," Science **256**, 66-70 (1992).

[5] O. Painter, R. K. Lee, A. Scherer, A. Yariv, J. D. O'Brien, P. D. Dapkus, and I. Kim, "Two-dimensional photonic band-gap defect mode laser," Science **284**, 1819-1821 (1999).

[6] C. J. M. Smith, H. Benisty, S. Olivier, M. Rattier, C. Weisbuch, T. F. Krauss, R. M. De La Rue, R. Houdré, and U. Oesterle, "Low-loss channel waveguides with two-dimensional photonic crystal boundaries," Appl. Phys. Lett. **77**, 2813-2815 (2000).

[7] Y.-G. Roh, S. Yoon, H. Jeon, S.-H. Han, and Q-H. Park, "Experimental verification of cross talk reduction in photonic crystal waveguide crossings," Appl. Phys. Lett. **85**, 3351-3353 (2004).

[8] T. Baba, "Slow light in photonic crystals," Nat. Photonics **2**, 465 (2008).

[9] S. John, and T. Quang, "Spontaneous emission near the edge of a photonic band gap," Phys. Rev. A **50**, 1764 (1994).

[10] J. P. Dowling, M. Scalora, M. J. Bloemer, and C. M. Bowden, "The photonic band edge laser: A new approach to gain enhancement," J. Appl. Phys. **75**, 1896

(1994).

[11] S. Kim, S. Ahn, K. Min, S. Kim, H. Jeon, P. Regreny, and C. Seassal, "Nano Stepping-Stone Laser," Appl. Phys. Express **6**, 042703 (2013).

[12] D. Y. Zhou and R. Biswas, "Photonic crystal enhanced light-trapping in thin film solar cells," J. Appl. Phys. **103**, 093102 (2008).

[13] C. M. Johnson, P. J. Reece, and G. J. Conibeer, "Slow-light-enhanced upconversion for photovoltaic applications in one-dimensional photonic crystals," Opt. Lett. **36**, 3990 (2011).

[14] Y. Park, E. Drouard, O. El Daif, X. Letartre, P. Viktorovitch, A. Fave, A. Kaminski, M. Lemiti, and C. Seassal, "Absorption enhancement using photonic crystals for silicon thin film solar cells," Opt. Express **17**, 14312 (2009).

[15] E. F. Schubert, *Light-Emitting Diodes* (Cambridge University Press 2006).

[16] R. Rossetti, S. Nakahara, and L. E. Brus, "Quantum Size Effects in the Redox Potentials, Resonance Raman-Spectra, and Electronic-Spectra of CdS Crystallites in Aqueous-Solution," J. Chem. Phys.**79**, 1086 (1983).

[17] C. B. Murray, D. J. Norris and M. G. Bawendi, "Synthesis and Characterization of Nearly Monodisperse CdE (E = S, Se, Te) Semiconductor Nanocrystallites," J. Am. Chem. Soc. **115**, 8706 (1993).

[18] M. A. Hines and P. Guyot-Sionnest, "Synthesis and characterization of strongly luminescing ZnS-Capped CdSe nanocrystals," J. Phys. Chem-Us. **100**, 468 (1996).

[19] B. O. Dabbousi, J. RodriguezViejo, F. V. Mikulec, J. R. Heine, H. Mattoussi, R. Ober, K. F. Jensen and M. G. Bawendi, "(CdSe)ZnS core-shell quantum dots:

Synthesis and characterization of a size series of highly luminescent nanocrystallites," J. Phys. Chem. B **101**, 9463 (1997).

[20] C. B. Murray, C. R. Kagan and M. G. Bawendi, "Synthesis and characterization of monodisperse nanocrystals and close-packed nanocrystal assemblies," Annu. Rev. Mater. Sci. **30**, 545 (2000).

[21] J. Lim, S. Jun, E. Jang, H. Baik, H. Kim and J. Cho, "Preparation of highly luminescent nanocrystals and their application to light-emitting diodes," Adv. Mater. **19**, 1927 (2007).

[22] K. S. Cho, E. K. Lee, W. J. Joo, E. Jang, T. H. Kim, S. J. Lee, S. J. Kwon, J. Y. Han, B. K. Kim, B. L. Choi and J. M. Kim, " High-performance crosslinked colloidal quantum-dot light -emitting diodes," Nat. Photonics **3**, 341 (2009).

[23] N. C. Anheier, "Colourful particles for spectrometry," Nature **523**, 39-40 (2015).

[24] P. Pust, V. Weiler, C. Hecht, A. Tücks, A. S. Wochnik, A.-K. Henß, D. Wiechert, C. Scheu, P. J. Schmidt and W. Schnick, "Narrow-band red-emitting $Sr[LiAl_3N_4]:Eu^{2+}$ as a next-generation LED-phosphor material," Nat. Mater. **13**, 891 (2014).

[25] H. Daicho, T. Iwasaki, K. Enomoto, Y. Sasaki, Y. Maeno, Y. Shinomiya, S. Aoyagi, E. Nishibori, M. Sakata, H. Sawa, S. Matsuishi and H. Hosono, "A novel phosphor for glareless white light-emitting diodes," Nat. Commun. **3**, 1132 (2012).

[26] W. B. Im, N. George, J. Kurzman, S. Brinkley, A. Mikhailovsky, J. Hu, B. F. Chmelka, S. P. DenBaars and R. Seshadri, "Efficient and Color-Tunable Oxyfluoride Solid Solution Phosphors for Solid-State White Lighting," Adv. Mater. **23**, 2300 (2011).

[27] C.-Y. Sun, X.-L. Wang, X. Zhang, C. Qin, P. Li, Z.-M. Su, D.-X. Zhu, G. -G. Shan, K. -Z. Shao, H. Wu and J. Li, "Efficient and tunable white-light emission of metal–organic frameworks by iridium-complex encapsulation," Nat. Commun. **4**, 2717 (2013).

[28] K. Min, Y.-K. Choi and H. Jeon, "Model calculations for enhanced fluorescence in photonic crystal phosphor," Opt. Express **20**, 2452 (2012).

[29] K. Min, S. Choi, Y. Choi and H. Jeon, "Enhanced fluorescence from CdSe/ZnS quantum dot nanophosphors embedded in a one-dimensional photonic crystal backbone structure," Nanoscale **6**, 14531 (2014).

[30] K. Min, H. Jung, Y. Park, K.-S. Cho, Y.-G. Roh, S. Hwang and H. Jeon, "A colloidal quantum dot photonic crystal phosphor: nanostructural engineering of the phosphor for enhanced color conversion," Nanoscale **9**, 8703 (2017).

[31] K.-M. Ho, C. T. Chan, and C. M. Soukoulis, "Existence of a photonic hap in periodic dielectric structures," Phys. Rev. Lett. **65**, 3152 (1990).

[32] R. D. Meade, A. M. Rappe, K. D. Brommer, J. D. Joannopoulos, and O. L. Alerhand, "Accurate theoretical analysis of photonic band-gap materials," Phys. Rev. B. **48**, 8434 (1993).

[33] K. S. Yee, "Numerical solution of initial boundary value problems involving Maxwell's equations in isotropic media," IEEE Trans. Antennas Propag. **14**, 302 (1996).

[34] P. Yeh, *Optical Waves in Layered Media* (Wiley 1988).

Chapter 2

Efficient White Light Generation using Photonic Crystal Phosphors

2.1 Introduction

Efficient white light sources have a tremendous impact as they are now demanded more than ever for various applications, including the backlights of display panels, automobile lamps, and general lighting systems [1-3]. In particular, white light-emitting diodes (LEDs) are expected to prevail soon over other types of white light sources due to many unique advantages they can offer, such as high energy efficiency, environmental friendliness, compact size, long lifetime, and durability [4-7]. Among different ways of constructing white LEDs, the most cost-effective and thus popular scheme is to combine a blue LED chip with one or more color-converting phosphors. In this context, phosphors are an ingredient of white LEDs as important as blue LED chips themselves [8-11]. Until now, however, most phosphor researches have focused on materials development, for example, to achieve a higher color-conversion efficiency or to adjust the absorption/emission bands to desired spectral ranges [12-15]. Although much progress has been made, phosphor developments through such conventional material-oriented approaches will be limited or saturated eventually. As a paradigm shift in phosphor

developments, our group have proposed and demonstrated a structural approach, that is, photonic crystal (PhC) phosphors [16-18].

By carving phosphor materials into a PhC structure and subsequently tuning the excitation photon energy to a PBE mode, where the photon group velocity becomes zero [19-22], we can relish a significantly strengthened interaction between excitation photons and phosphor materials and thus an improved color conversion efficiency (regardless of phosphor materials employed). Recently, our group reported enhanced color conversion efficiency from 1D lateral PhC phosphor, a thin-film one-dimensional (1D) PhC structure composed of alternately arranged dense CQDs (as a fluorescing low index material) and Si_3N_4 (as a passive high index material) [18]. In this chapter, I proposed an efficient white light generation method using the structurally engineered lateral 1D PhC phosphors (prepared from both red and green CQDs) on top of a blue LED chip. In comparison with the reference phosphor structure, which is composed of homogeneous (or structure-less) CQD films, the PhC phosphors result in a much higher luminance (with good chromaticity coordinates and color-temperature) even with a substantially reduced amount of CQDs. This observation indicates that the PhC phosphor is not just a conceptual advancement, but also a viable technology for next-generation white LEDs and their applications.

2.2 Device design and Numerical Analyses

2.2.1 Photonic band structure of lateral 1D photonic crystals

I first examined the photonic band structure of the lateral 1D PhC structure using the FDTD method [23]. The lateral 1D PC phosphor structure is composed of two materials with refractive index of $n_H = 2.05$ (for high index materials) and $n_L = 1.82$ (for low index materials), which are the typical refractive indices of silicon nitride and red CQDs, respectively. Figure 3-2-1(a) shows a schematic of the lateral 1D PhC phosphor structure. The period of the structure is given by $\Lambda = 280$ nm and filling factor of QDs in each period is 50 %, which means $d_H = d_L = 140$ nm. The unit cell of the lateral PhC structure used in FDTD simulation is shown in Fig. 3-2-1(b). I set the *x*-axis parallel to direction of the periodicity and the *z*-axis is the vertical axis to surface.

Figure 2-2-2 shows the photonic band structure of the lateral 1D PhC and corresponding electric field profiles of PBE modes. The band structure we obtained is dispersion relation of photons in 1D PhCs and there are two kinds of symmetric points where $k_x = 0$ and $k_x \neq 0$. Where k_x is the wave vector in direction of periodicity. In all of PBE modes I calculate, electric fields confined in the PhC phosphor slab so the increase of light-matter interaction by PBE effect seems to be valid. However, an important factor for efficient pumping is not only confinement of electric fields at PBEs but also coupling of external pump photons to PBE modes. Figure 2-2-3 displays directions of wave vector **k** of PBE modes at each symmetric point. In case of $k_x \neq 0$, direction of vector **k** is vertical to propagation direction of pump photons and there is no coupling to PBE modes. On the other hand, in case of $k_x = 0$, wave vector **k** and propagation of pump photons have the same direction and

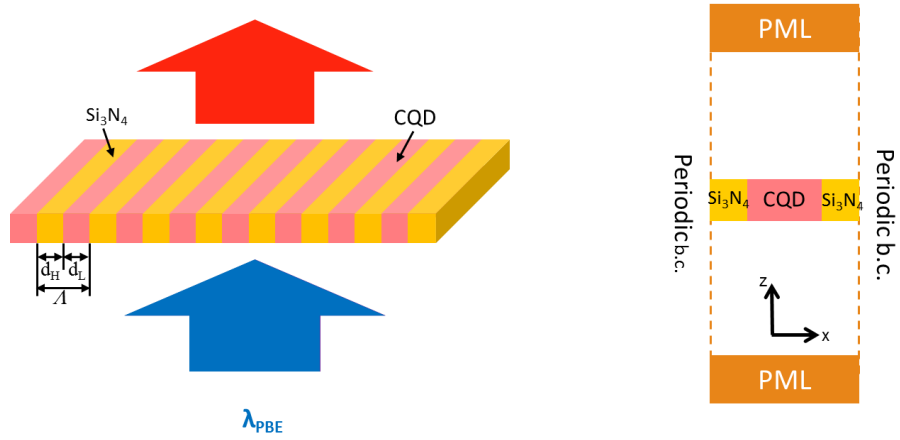

Figure 2-2-1 (a) Schematic of the lateral 1D PhC phosphor structure composed of silicon nitride and CQDs. (b) A schematic of unit cell of the lateral 1D PhC structure, in which FDTD simulations are performed to calculate photonic properties of the lateral 1D PhC.

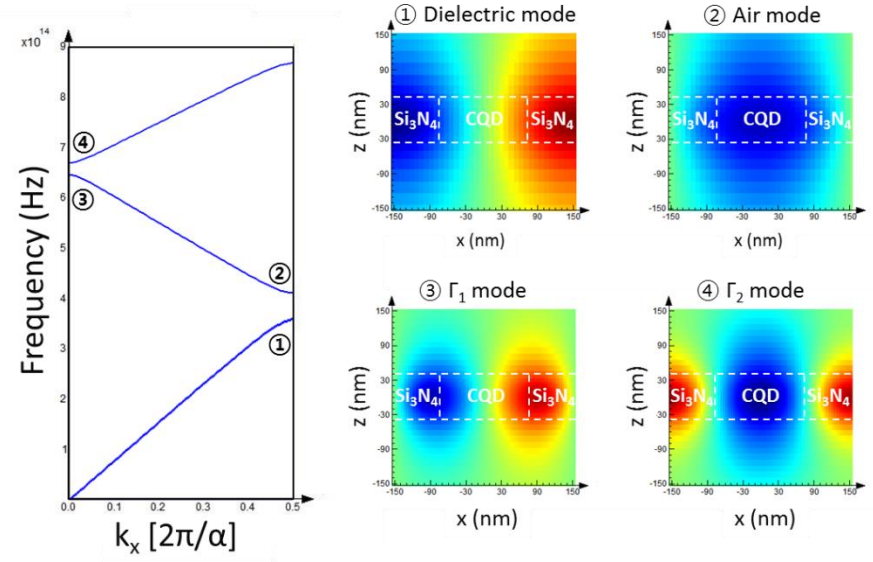

Figure 2-2-2 Photonic band structure of the lateral 1D PhC and corresponding electric field profiles of PBE modes in case of $k_x \neq 0$ (①,②) and $k_x = 0$ (③,④).

coupling of pump photons and PBE modes occurs.

Since the Γ point generally refers to a symmetric point with no lateral component of the wave vector of the slab waveguide, the symmetry point with kx = 0 is also referred to as Γ point in this thesis [24].

Next, the FDTD simulation of the lateral 1D PhC phosphor structure including a glass substrate with refractive index of ~1.52 was performed. As shown in Figure 2-2-4, the photonic band structure of the lateral 1D PhC having a glass substrate is similar to that of the lateral 1D PhC without a substrate except for narrowing the PBG width due to the change of the effective refractive index of the structure.

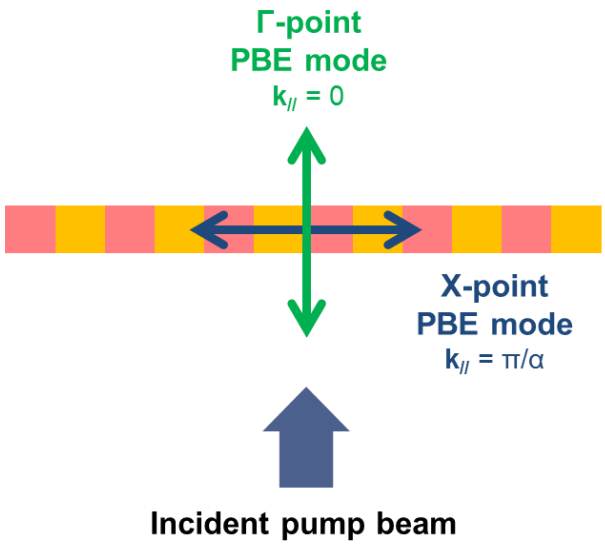

Figure 2-2-3 Directions of wave vector **k** of PBE modes at each symmetric point.

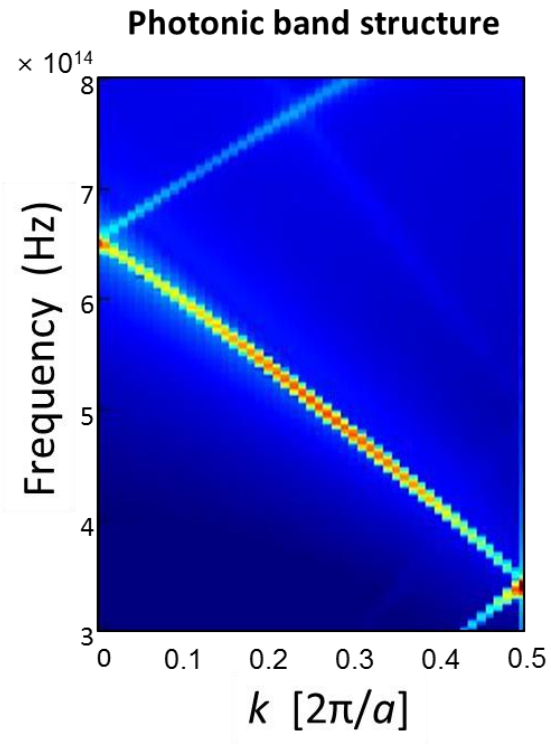

Figure 2-2-4 Photonic band structure of the lateral 1D PC with a glass substrate.

2.2.2 Absorption enhancement

Finite-difference time-domain (FDTD) simulations were performed to predict the performance characteristics and also to find the optimum structures of the PhC phosphors. The photoluminescence (PL) enhancement at the Γ-point PBE of the lateral 1D PhC phosphor was evaluated by calculating the absorbance of the pump photon in the PhC structure under the assumption that the IQE of the phosphor is unity. This is a constant assumption within this thesis.

Absorbance per unit volume obtained from the divergence of the Poynting vector [25] is given by

$$\text{Absorbance} = -\frac{1}{2}\cdot \text{real}\left(\vec{\nabla}\cdot\vec{P}\right),$$

which formula can be rewritten as

$$\text{Absorbance} = -\frac{1}{2}\cdot \text{real}\left(i\omega\vec{E}\cdot\vec{D}\right).$$

With more simplifications, we get results that are suitable for use in simulation

$$\text{Absorbance} = -\frac{1}{2}\cdot \omega|E|^2\text{imag}(\varepsilon).$$

These processes and results are provided in the Lumerical FDTD solution, the commercial computer software product used in this chapter [23].

Refractive indices of Si_3N_4 and dense CQDs were obtained from spectroscopic ellipsometry measurements on independently prepared films, while the data book by Palik [26] was consulted for fused quartz substrate. The complex refractive indices ($n + ik$) of the CQD films at the peak wavelength of the blue LED chip used (λ = 450 nm) are 1.82 + 0.024i for the red CQDs and 1.92 + 0.149i for the green CQDs,

respectively. The simulation model structures are constructed based on the actual SEM images shown in Figure 2-2-5 (a) with a special attention given to the surface morphology profiles. The thickness (t = 90 nm) and the duty-cycle (50%) of the Si_3N_4 grating are fixed, while the grating period is varied in the vicinity of Λ = 280 nm. Figure 2-2-5 shows cross-sectional SEM image of the PhC phosphor after CQD coating (a) and modeling structure of the PhC phosphor, where cross-section structure and the groovy surface morphology are reflected, and Λ, the period of 1D PhC is also indicated (b).

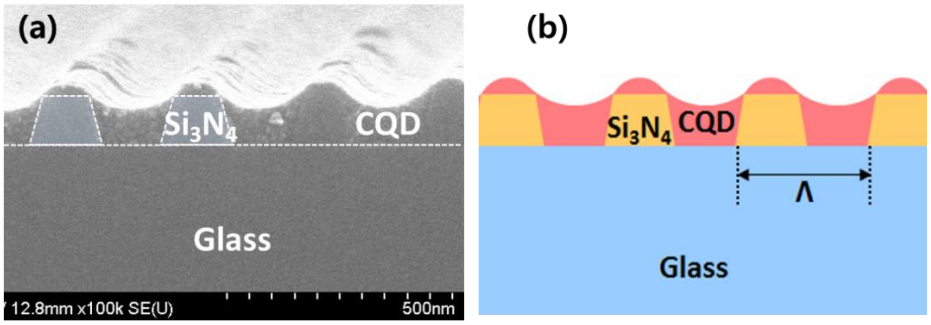

Figure 2-2-5 PhC phosphor structure. (a) Cross- sectional SEM image of the PhC phosphor (b) Schematic of a 1D PhC phosphor with CQD coated.

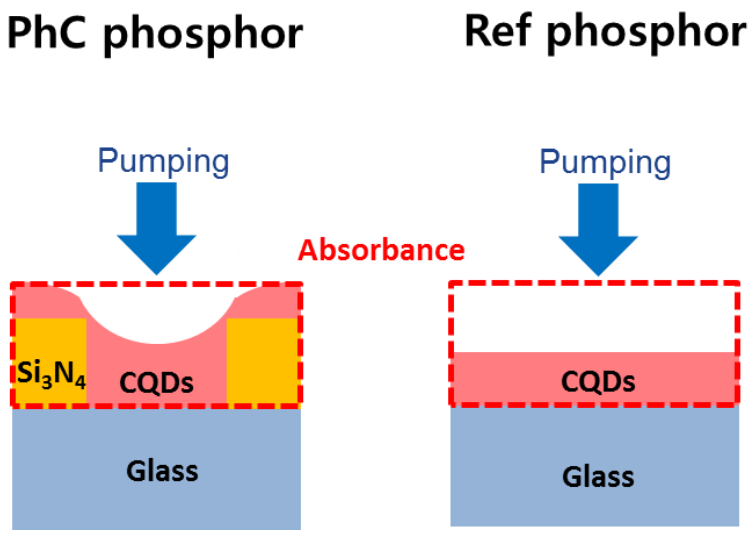

Figure 2-2-6 Unit cells of the lateral 1D PC phosphor with the glass substrate (left) and reference phosphor (right).

It should be reminded that despite the ample difference in emission wavelengths, the 1D PhC structures (thus their PBE modes) of the both red and green PhC phosphors are basically the same because their intended resonances are for excitation (by the blue LED chip), not for emission (from the red or green CQDs). Shown as functions of excitation wavelength in Figure 2-2-6 (a) and (b) are CQD absorbance spectra simulated for the red and green PhC phosphors, respectively, for a few different grating periods (Λ). In each case, one can clearly see a strong resonance peak. The resonance wavelength λ_0, which corresponds to the band-edge mode at the 1D PhC zone center [18], changes in response to the grating period, thus provide a convenient means of tuning the excitation resonance wavelength. The sensitivities estimated from the simulation results are $\Delta\lambda_0/\Delta\Lambda \approx 1.4$ for PhC phosphors. Although the grating structures are very similar (in terms of period and duty-cycle), the resonance details such as the widths and absolute values of absorbance are quite different for the red and green PhC phosphors, which is due to the difference in the complex refractive indices of the two kinds of CQDs. In large contrast, the reference phosphors exhibit no special feature in the absorbance spectra except for the gradual and monotonic change, which reflects simple dispersion characteristics of the CQD materials.

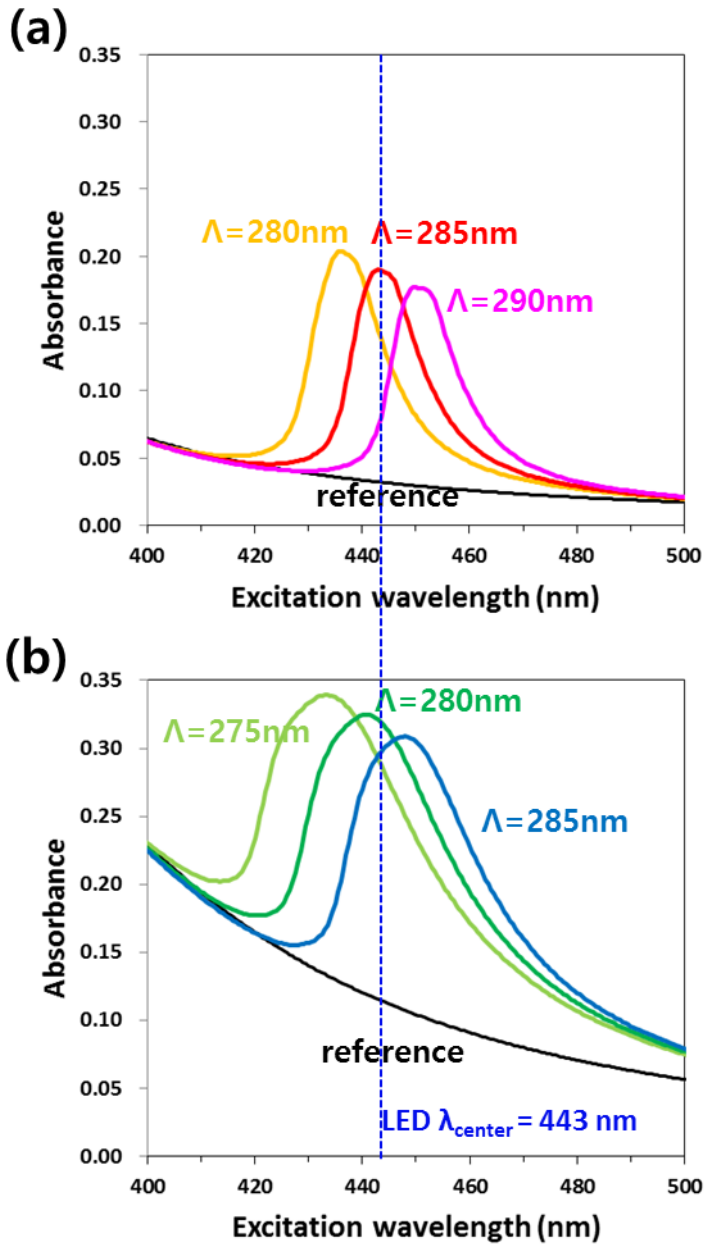

Figure 2-2-7 Calculated CQD absorbance spectra of the red (a) and green (b) PhC phosphors for a few different grating periods.

Figure 2-2-7 (a) and (b) are the absorbance enhancement factor spectra for the corresponding PhC phosphors, which is obtained by taking the absorbance ratio between the PhC phosphor and the reference phosphor at a given excitation wavelength. We show the results only for particular PhC phosphor structures (Λ = 285 nm for the red CQDs and Λ = 280 nm for the green CQDs) because they exhibit resonances at $\lambda \approx$ 443 nm, the center wavelength of the blue LED chip that we will use later as the excitation source for white light generation. The peak enhancement factors are as high as ~5.9 and ~3.3 for the red and green PhC phosphors, respectively. It should be worth noting that as the excitation wavelength goes away from the resonance the enhancement factor converges to the unity for the both PhC phosphors. This is not only a direct proof that the PhC effect vanishes but also an indirect evidence that the CQD volume in the PhC phosphor is equal to that in the reference phosphor.

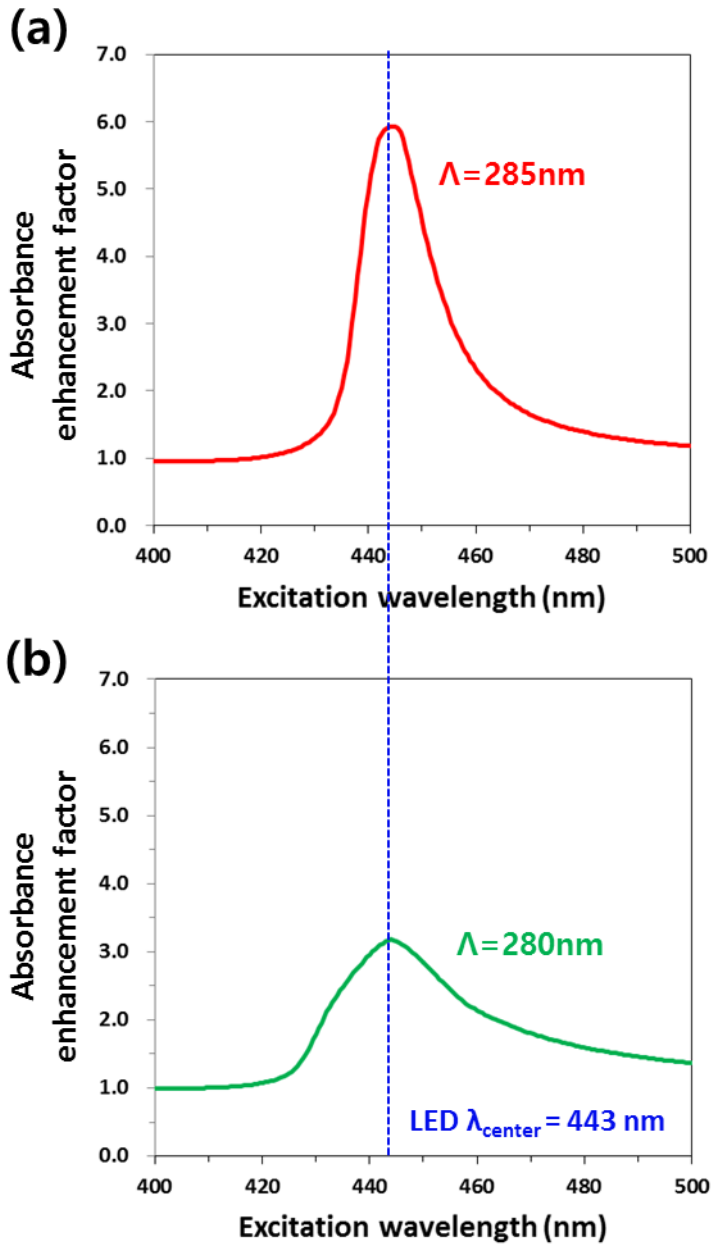

Figure 2-2-8 Absorbance enhancement factor spectra for the red (a) and green (b) PhC phosphors.

2.3 Sample Fabrication

2.3.1 Laser holographic lithography

Various patterning methods can be used to construct 1D lateral PhC phosphor, for example, electron beam lithography, photo lithography, and laser holographic lithography (LHL). After 1D grating pattern is formed on the thin film, a dry or wet etching process is performed to transfer the pattern to the thin film to produce a PhC structure. Table 3-1-1 shows comparison between three generally used lithography methods. Since the PhC phosphors are designed for use in light-emitting devices, we need a large area patterning method with sub-micron spatial resolution. While electron beam lithography offers very high spatial resolution, it is a tedious and costly process for large area patterning. In photolithography method, using an opaque plate as a photomask, pattern is written quickly in a large area but the spatial resolution is lower than other lithography methods. LHL can be used for large area patterning and offers sub-micron spatial resolution [27,28]. I employed LHL to fabricate the lateral PhC phosphors [29,30].

The basic principle of LHL is very similar to those of optical interferometer. Fig. 3-3-1(a) shows our setup for LHL. Electromagnetic waves emitted from a 266-nm diode-pumped solid-state (DPSS) laser are expanded by an objective lens, almost becoming planar waves near the sample stage. Two coherent planar lights, one directly from the objective lens and the other reflected from the mirror generate interference pattern as can be seen in Fig. 3-3-1(b). After post-exposure bake and develop process, photoresist (PR) pattern corresponding to the periodic intensity pattern of incident light are generated. The period of the periodic pattern is given by

$$\text{Period} = \frac{\lambda}{2\sin\theta}$$

where λ is the laser wavelength (= 266 nm) and θ is the angle of rotation of the sample stage [31].

I used negative PR (AZ nlof 2070, Electronic materials) for the LHL process and Figure 2-3-2 shows the shape of the PR pattern with exposure time. In the case of fabrication of the lateral 2D PC phosphors, we only need to perform one more LHL step on the 90˚-rotated samples [32].

	E-beam lithography	**Photo-lithography**	**LH lithography**
Cost	high	high	low
Throughput	low	high	high
Large-area	X	O	O
Mask	X	O	X
Minimum feature size	~ 10 nm	~ few μm	~ 100 nm
Flexibility	O	O	X (only periodic patterns)

Table 2-3-1 Comparison between three generally used lithography methods.

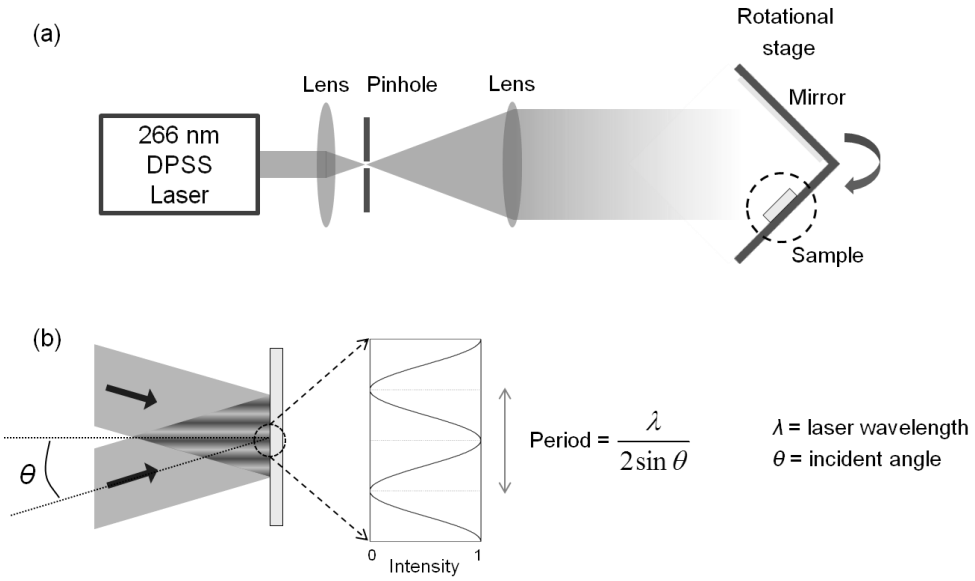

Figure 2-3-1 (a) Schematic diagram of laser holographic lithography setup using 266 nm DPSS laser as a light source. (b) Interference pattern consisting of a periodic series of fringes representing intensity maxima and minima [33].

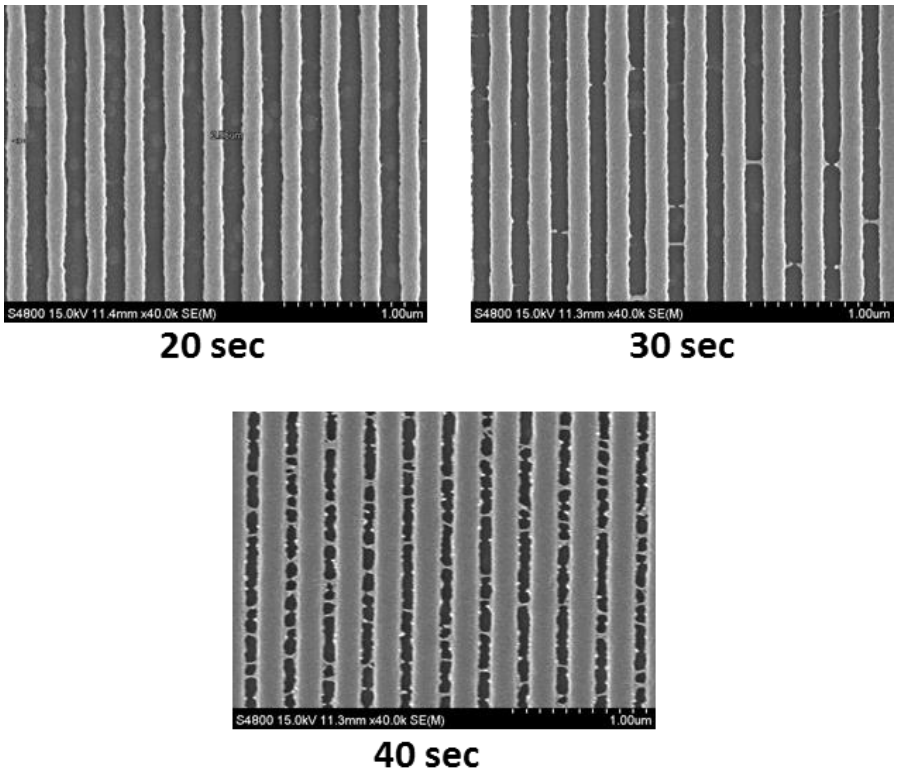

Figure 2-3-2 SEM images of PR pattern fabricated by LHL with exposure time.

2.3.2 Fabrication steps

Figure 2-3-2 shows the step of fabrication processes. Fabrication was begun with the deposition of a 90-nm-thick Si_3N_4 film on a 1 cm × 1 cm glass substrate using plasma-enhanced chemical vapor deposition (PECVD) (310PC, Surface Technology Systems). PR grating pattern for a 1D PhC structure was generated by LHL, as shown in Figure 2-3-3 (a). PR grating pattern was subsequently transferred down to the underlying Si_3N_4 layer using reactive-ion etching (RIE) (Plasmalab 80 Plus, Oxford Instruments). The etching selectivity of Si_3N_4 on SiO_2 was improved during the RIE process by addition of N2 gas [34]. Figure 2-3-3(b) represents a SEM image of the lateral 1D PhC backbone for the phosphor structure. CdSe-based CQDs, synthesized chemically and dispersed in cyclohexane solution in 1.0 wt%, were then spin-coated at 2000 rpm for 30 seconds to form a densely packed CQD layer on top of the 1D Si_3N_4 grating. Figure 2-3-3(c) shows a SEM image of a cross section of the QD-coated PhC phosphor sample. For comparison, CQDs were spin-coated on a flat glass substrate to produce a reference phosphor. Figure 2-3-4 shows cross-sectional scanning electron microscope (SEM) images of a typical PhC phosphor (before and after the CQD coating) as well as a reference phosphor prepared on flat substrate. Note that the PhC phosphor is characterized by a groovy surface morphology that is partially conformal to the underlying grating structure whereas the reference phosphor is planar. Careful examination on the SEM images indicates that the average thickness of CQD of PhC phosphor is 54 nm, which is very close to that of reference phosphor (~ 55 nm). So CQD fluorescence data obtained from the two kinds of phosphor structures can be directly compared (*i.e.*, without normalization by the CQD quantities).

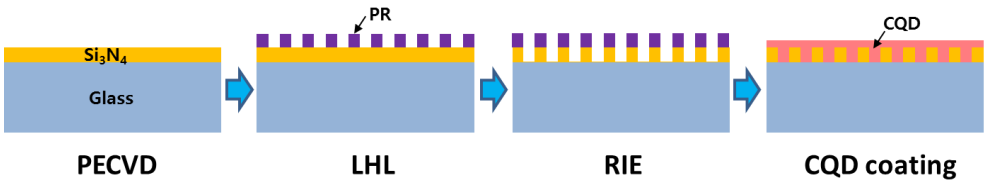

Figure 2-3-3 Schematic diagram of fabrication steps. (1) A silicon nitride layer was deposited by plasma-enhanced chemical vapor deposition (PECVD) on a glass substrate. (2) Laser holographic lithography (LHL) was applied to generate 1D PhC patterns to PR. (3) The patterned sample was dry-etched using reactive-ion etching (RIE) method. (4) QDs were spin-coated on the sample to construct the lateral PhC phosphor.

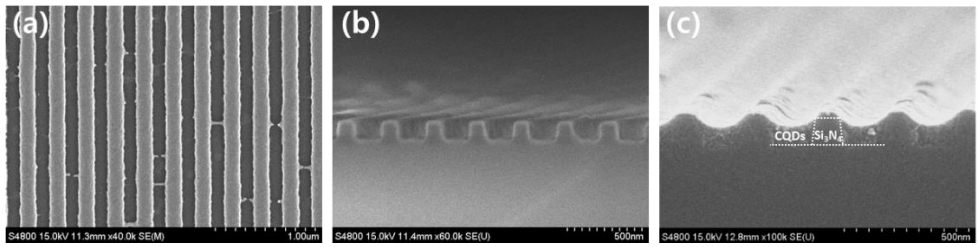

Figure 2-3-4 SEM images of fabricated 1D PCs. (a) Top view of patterned photoresist on the silicon nitride layer. (b) Side view of the dry-etched silicon nitride patterned layer. (c) Side view of the QD-coated PhC phosphor sample.

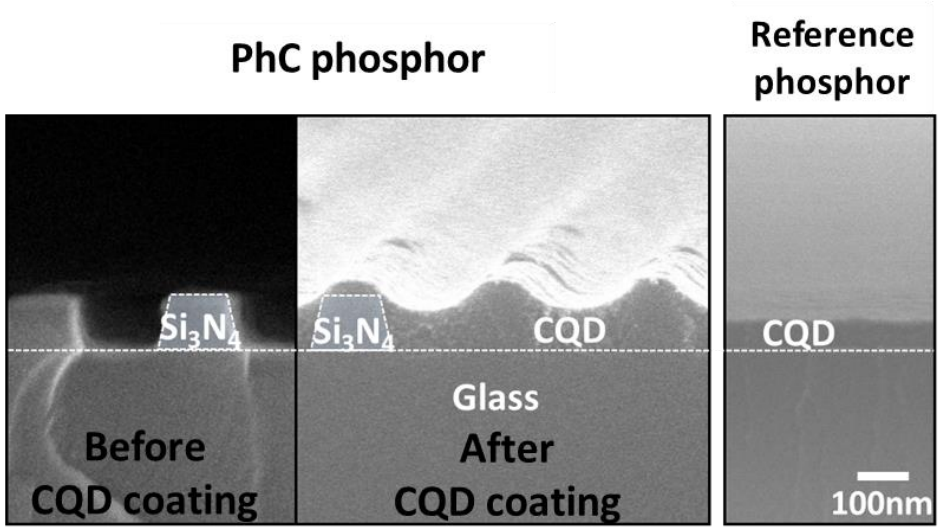

Figure 2-3-5 Cross-sectional SEM image of the PhC phosphor plate before and after CQD coating. (left) and the reference phosphor plate (right), the boundaries of CQD and Si_3N_4 are also shown for clarity (white dashed line).

To generate high quality white light starting from a blue LED chip ($\lambda_B \approx 450$ nm), we need additional colors of red and green [8,35]. So we prepared two kinds of CQDs, one emitting in red ($\lambda_R \approx 620$ nm) and the other in green ($\lambda_G \approx 530$ nm; the red CQDs we used have a CdSe–CdS–ZnS core–shell–shell structure while the green CQDs are composed of CdSeS alloy core and ZnS shell [36-38]. Shown in Figure 2-3-5 are photographs of four different phosphor plates in a matrix format: two PhC phosphors with red and green CQDs in the left and two reference phosphors with red and green CQDs in the right, all taken at once under a directional illumination condition. Note that the images of the two PhC phosphors are dominated by strong iridescence, both exhibiting identical green colors; this is because the two kinds of PhC phosphors possess nominally identical grating

structures to make the band-edge mode tuned at the blue excitation wavelength (regardless of the CQDs employed). In good contrast, the reference phosphors exhibit no sign of diffraction (because of the lack of any grating structure), but only faint fluorescence colors from the corresponding CQDs.

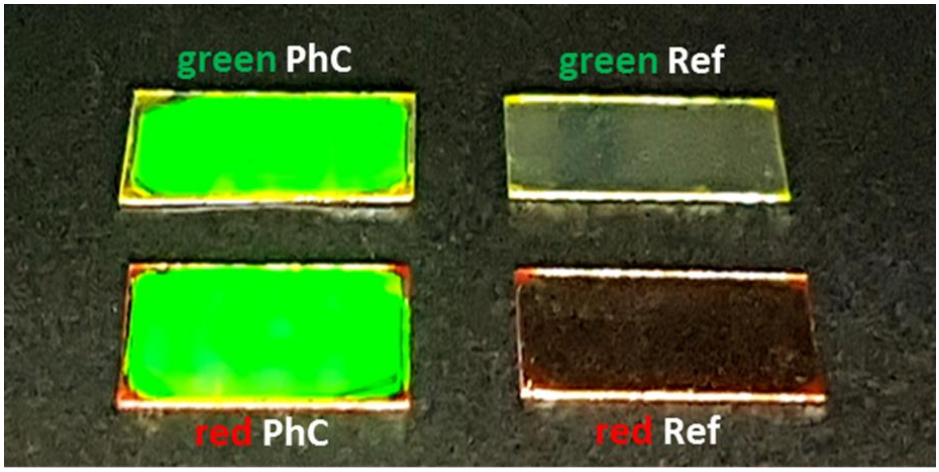

Figure 2-3-6 Photograph images of PhC phosphors (left) and reference phosphors (right) with green (upper) and red (lower) CQD coated.

2.4 Measurement and Analyses

2.4.1 Photoluminescence measurement setup

To investigate properties of the individual PhC phosphors, I performed photoluminescence (PL) excitation experiments using a tunable excitation source, in which the excitation wavelength was scanned across the intended excitation resonance at λ = 443 nm. Figure 2-4-1 shows schematic of PL measurement set up. We combined a Xe lamp (6271 Xenon arc lamp, Newport) with a monochromator (DK240, Spectrum) to create a wavelength-tunable excitation source with a wide tuning range. A polarizer was inserted between the exit slit of the monochromator and sample to control the polarization status of the excitation beam. The monochromator slit width was adjusted so that the spectral linewidth was ~2 nm full width at half maximum (FWHM), which is sufficiently narrow to resolve any detailed spectral feature appearing in the PL spectra. PL spectra were measured in transmission geometry, where the excitation beam was incident directly onto the CQD surface and the PL spectra were taken through the glass substrate using a spectrometer (iHR320 spectrometer, Horiba Jobin Yvon). All PL measurements were made at room temperature.

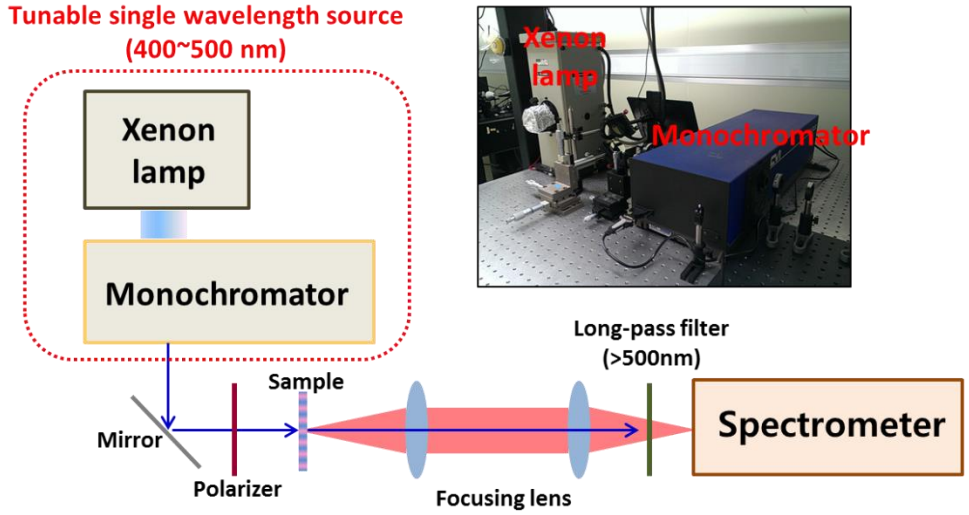

Figure 2-4-1 PL measurement setup with a wavelength-tunable monochromatic light source to characterize PL intensity from phosphor structures.

2.4.2 Photoluminescence measurement and enhancement factor

Figures 2-4-2(a) and 2-4-2(b) show the PL spectra measured for the red reference phosphor and the red PhC phosphor, respectively. PL spectra remain unchanged in terms of their peak wavelengths (~615 nm), as well as spectral linewidths (~35 nm in FWHM), regardless of the excitation wavelengths. As the excitation wavelength changes, the reference phosphor showed little change in PL intensity. In contrast, the PL intensity varies considerably in PhC phosphor.

Figure 2-4-3 represents the PL intensity spectra of the red PhC phosphor and the red reference phosphor together, which intensities are integrated values at each excitation wavelengths. By obtaining the PL intensity ratio of the lateral PhC phosphor to that of the reference phosphor, which is called to the PL enhancement factor, I could consider the PBE effect only. Shown in Fig. 2-4-4 is the PL enhancement factor which is obtained by taking the PL intensity ratio between the PhC phosphor and the reference phosphor. For comparison, absorbance enhancement factor calculated in section 2.2.2 is shown in the inset. Table 2-4-1 compares PBE wavelengths and enhancement factor of measurement data and calculated data. The results of experiments agree well with numerical calculation. The maximum PL enhancement factors (~5.5) are slightly lower than the simulated absorbance enhancement factors (~5.9), which we attribute to the internal quantum efficiencies of the CQDs that can never be the unity.

The green PhC phosphors was also tested by the same procedure as in the case of red, and the results are shown in the Figure 2-4-5, Figure 2-4-6, Figrue 2-4-7 and Table 2-4-2. The smaller enhancement factor of green PhC phosphor than red PhC phosphor result from the smaller refractive index difference with Si_3N_4

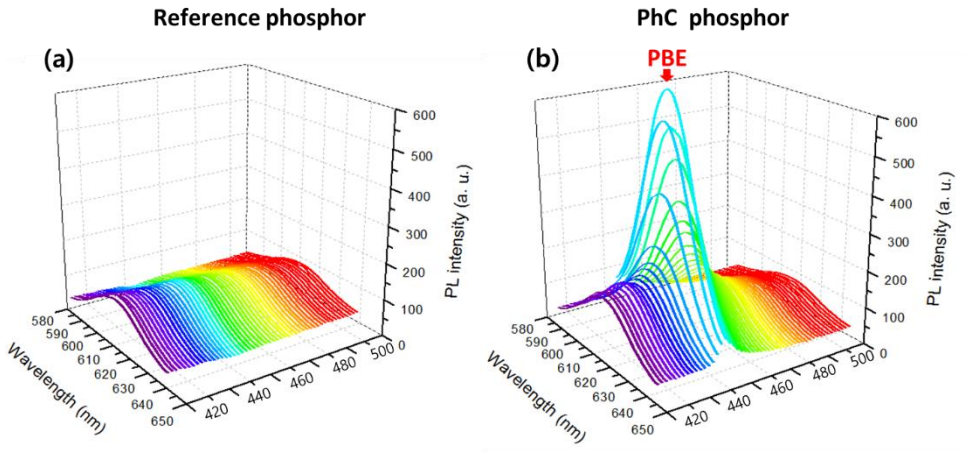

Figure 2-4-2 PL spectra measured as a function of excitation wavelength: the red reference phosphor (a) and the red PhC phosphor (b).

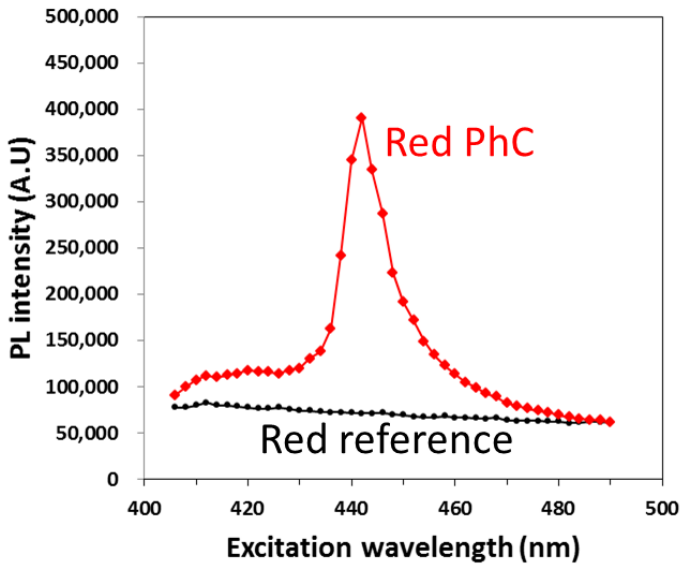

Figure 2-4-3 Integrated PL intensity spectra of the red PhC phosphor and the red reference phosphor.

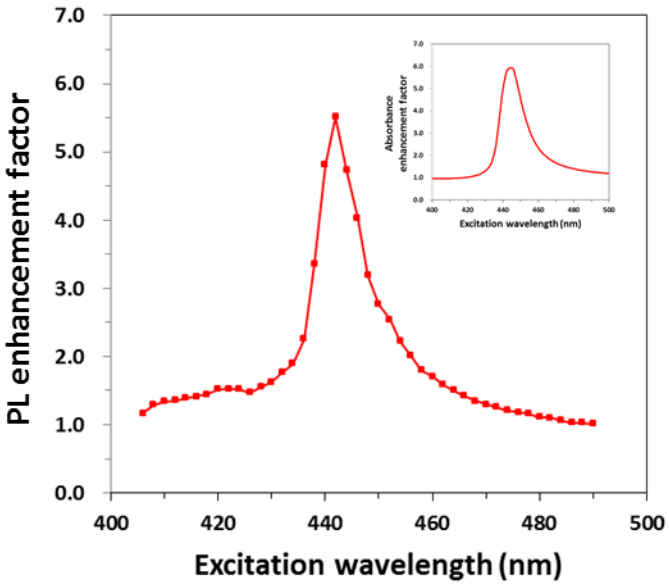

Figure 2-4-4 PL enhancement factor of the red PhC phosphor. Inset: calculated absorbance enhancement factor.

red	**PBE wavelength**	**Enhancemet factor**
Measurement	442 nm	5.9
Simulation	444 nm	5.5

Table 2-4-1 Comparison of measurement data and calculated data.

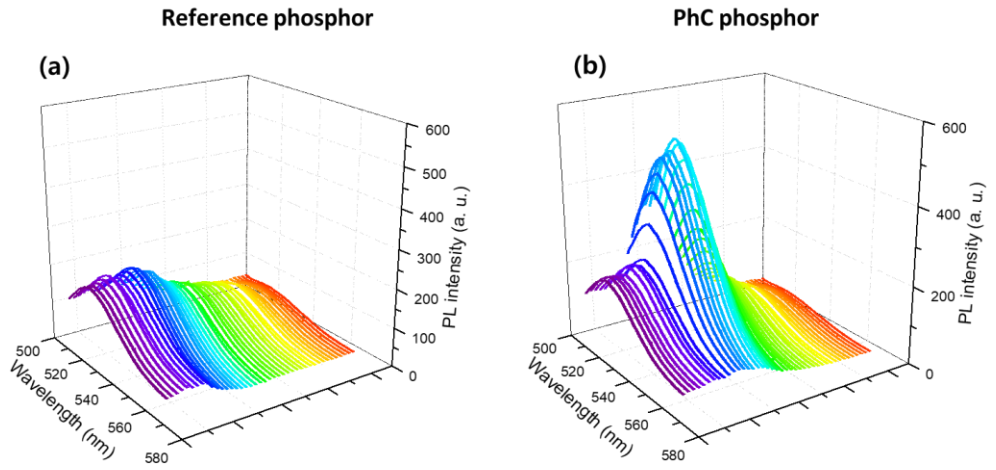

Figure 2-4-5 PL spectra measured as a function of excitation wavelength: the green reference phosphor (a) and the green PhC phosphor (b).

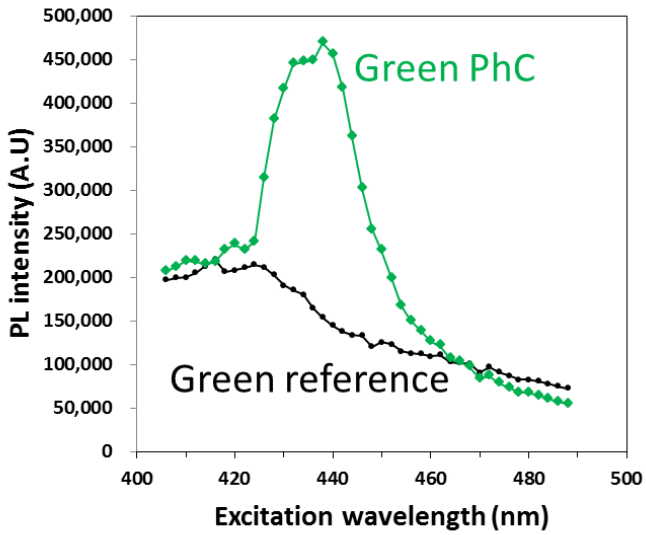

Figure 2-4-6 Integrated PL intensity spectra of the green PhC phosphor and the green reference phosphor.

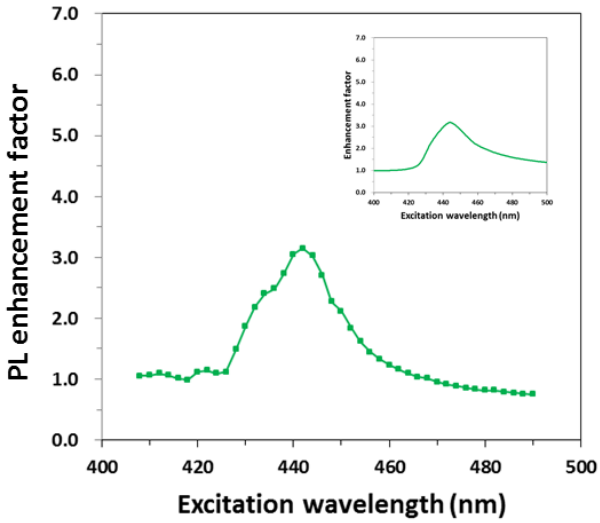

Figure 2-4-7 PL enhancement factor of the green PhC phosphor. Inset: calculated absorbance enhancement factor.

green	**PBE wavelength**	**Enhancemet factor**
Measurement	442 nm	3.1
Simulation	443 nm	3.2

Table 2-4-2 Comparison of measurement data and calculated data.

2.4.3 Polarization dependence of 1D PhC phosphors

Figure 2-4-8 intuitively show that the PBE effects in the lateral 1D PhC phosphors depend on the polarization of the excitation source. Electric fields are naturally perpendicular to the direction of propagation of electro-magnetic waves. Thus, if an external excitation photon incident perpendicularly to the surface of a 1D PhC phosphor, the direction of the electric field should be in the x-axis or the y-axis directions. And the direction of wave vectors of the PBE mode of the lateral 1D PhC is parallel to periodicity (perpendicular to grating directioin), so the direction of the electric field of PBE mode shuld be in the y-axis or the z-axis directions. In order to satisfy both conditions, the polarization direction of the excitation photon must be in the y-axis direction. Next, we conducted tests with a polarized excitation source to verify that the polarization of the excitation source affects the PL intensity of the lateral 1D PC phosphor. Figure 2-4-9 shows PL enhancement factor of the red lateral PC phosphor structures, when polarization angles of the excitation source are 0˚ and 90˚, respectively. In case that the angle of polarization is 0˚, which means direction of excitation source polarization is parallel to grating direction of the lateral 1D PhC, PL enhancements at corresponding PBE wavelengths occurred. On the other hand, no specific peaks appeared when the polarization angle of excitation source is 90˚. This is important evidence for the polarization dependence of the PBE effect of 1D PC phosphors, which means that PBE effect appears only when the excitation source is properly polarized.

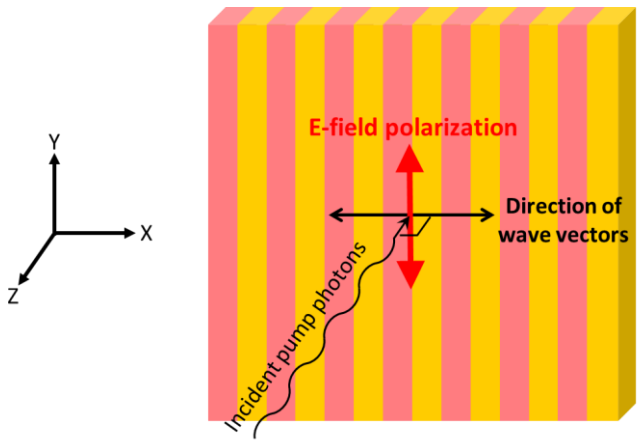

Figure 2-4-8 Polarization dependence of the photonic band-edge effect in the lateral 1D PhC.

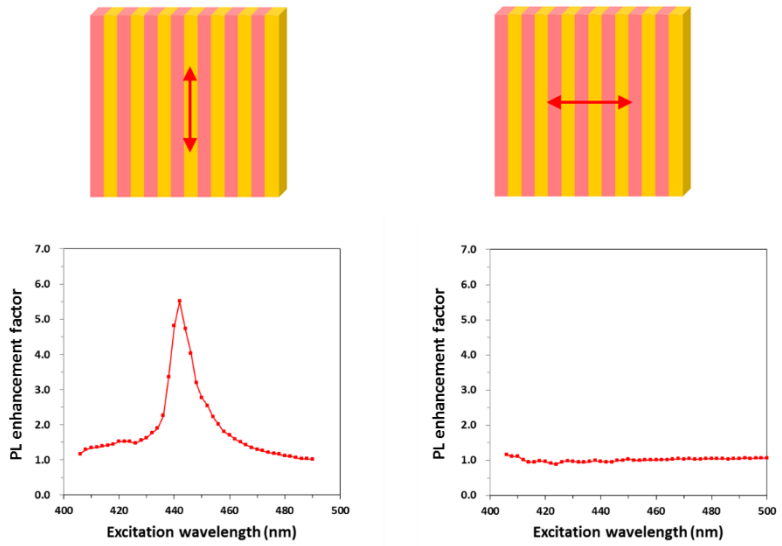

Figure 2-4-9 PL enhancement factor of the red lateral 1D PhC phosphor structure, when polarization angles of the excitation source are 0˚and 90˚.

2.4.4 Integrating sphere

The integrating sphere is an optical instrument for measuring luminous flux, luminous intensity, reflectance, etc. It is a hollow spherical cavity with its inner surface coated with a lambertian reflect material, with small holes for input and output ports. Before describing the operating principle of the integrating sphere, the units used for optical measurement are summarized in Table 2-4-3.

If the light source with a luminous intensity of 1cd is emitting in all directions, the luminous flux is,

$$\text{Luminous flux} = 4\pi \text{ lm}$$

and the illuminance at a distance d,

$$\text{Illuminance} = \frac{4\pi}{4\pi d^2} = \frac{1}{d^2} \text{ lux}$$

Thus, the relationship between the luminous intensity and the illuminance at distance d is,

$$\text{Illuminance} = \frac{\text{Luminous intensity}}{d^2} \cdots (1)$$

Figure 2-4-10 represents the relationship between luminous intensity and luminance at several reflection angles in the case of a labertian reflector.

In the case of a lambertian reflector, the luminance is constant at all angles and the relationship between luminous intensity and luminance at any angle is,

$$\text{Luminous intensity} = \text{Luminance} \times cos\boldsymbol{\Phi} \times \boldsymbol{A} \cdots (2)$$

Photometric unit	**Dimension**	**Meaning**
Luminous flux	lm	Amount of light in all directions
Luminous intensity	lm./sr = cd	Amount of light per unit solid angle
Illuminance	lm/m^2	Luminous flux per unit area
Luminance	$lm/(sr*m^2) = cd/m^2$	Luminous intensity per unit area

Table 2-4-3 Dimension and meaning of Photometric units [1].

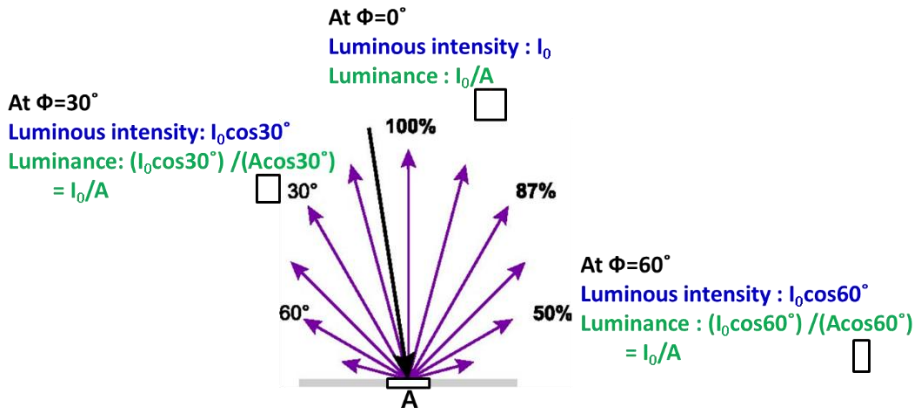

Figure 2-4-10 Relation between luminous intensity and luminance at several reflection angles in the case of a lambertian reflector.

In Figure 2-4-11, assuming that the luminance of the light reflected by the area ds of the point P is L, the light intensity Ip_1 in the direction from the point P to the direction P1 is,

$$I_{P_1} = \mathrm{L} \times ds \times cos\boldsymbol{\Phi} \quad by\ (2)$$

On the other hand, at a point p_1, an illuminance Ep_1 is,

$$E_{P_1} = \left({}^{I_{P_1}}\!/_{d^2} \right) \times cos\boldsymbol{\Phi} = \frac{(\mathrm{L} \times ds \times cos^2\boldsymbol{\Phi})}{d^2} = \frac{(\mathrm{L} \times ds)}{4r^2} \quad by\ (1)$$

That is, the illuminance is constant at any point in the integrating sphere.

If the illuminometer is located on any point of inner surface of integrating sphere and the illuminance of the illuminometer is E and the reflectance of the surface of the integrating sphere is R,

$$E = E_1 + E_2 + \cdots + E_n + \cdots = E_1(1 + R + \cdots + R^n) = E_1/(1 - R)$$

So the luminous flux is,

$$E \times (1 - R) \times 4\pi r^2$$

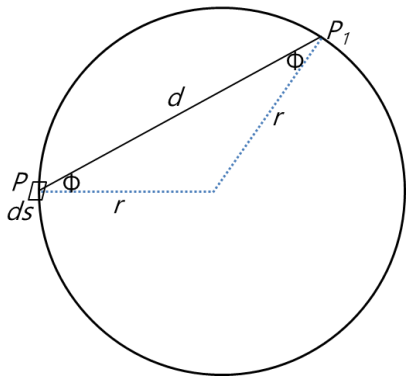

Figure 2-4-11 Schematic of integrating sphere

2.4.5 Spectrum measurement

To account for total emission from the system composed of a blue LED chip and the PhC phosphors, I constructed a simple evaluation stage where phosphor plates can be conveniently stacked on top of a blue LED chip, which in turn is inserted into an integrating sphere (the inner diameter 6”). The experimental setup is schematically depicted in Fig. 2-4-12. Total emission (red-green-blue) from the sample assembly is reflected by the inner surface of the integrating sphere and collected by a lens-capped fiber bundle and fed to a spectrometer (HR4000CG, Ocean Optics). The interior surface of the integrating sphere is coated with $BaSO_4$, excellent lambertian reflector. Before stacking the red and green PhC phosphors in a multiple, we evaluated their performances separately. Figure 2-4-13 and Figure 2-4-14 show the emission spectra from a single red and green PhC phosphor plate, respectively, while the blue LED is driven at constant DC current (50 mA); each figure also contains the emission spectrum from a single reference phosphor plate composed of the corresponding CQDs. When compared with the reference phosphors, the PhC phosphors exhibit enhanced CQD emission and simultaneously reduced blue LED emission (*i.e.*, enhanced absorption of the blue light) for the both red and green CQDs. Inset are the magnified spectra near the CQD emission peaks. The peak intensities of the PhC phosphors are ~2.0 and ~1.7 times higher for the red and green CQDs, respectively, than those of the reference phosphors. These enhancement factors, although significant, are much lower than the values obtained from the previous PL excitation experiments. However, one should note that a blue LED chip is a far less ideal excitation source than the one used in the photoluminescence excitation experiments; light from a blue LED chip is neither monochromatic, nor polarized, nor planar, nor perpendicular to the sample.

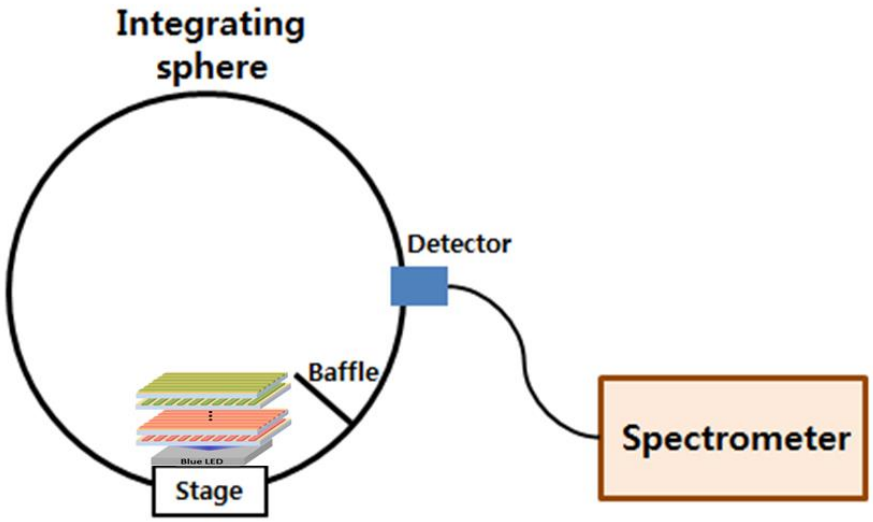

Figure 2-4-12 Schematic of integrating sphere setup for spectrum measurement.

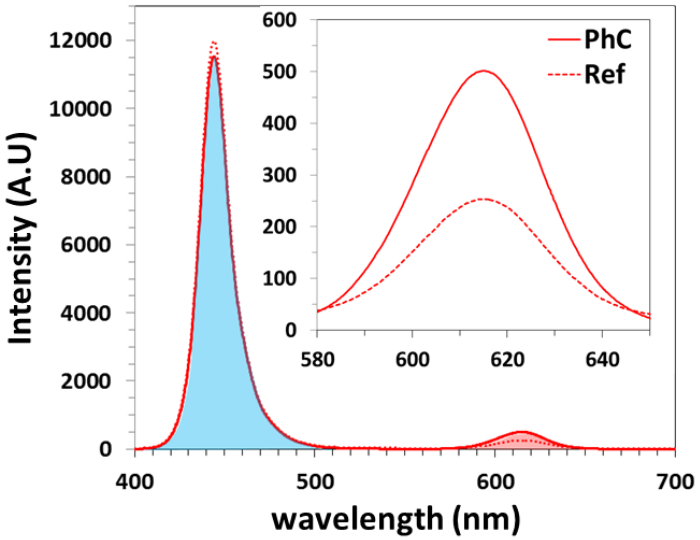

Figure 2-4-13 Measured spectra of single red PhC phosphor plate compared with a reference phosphor plate.

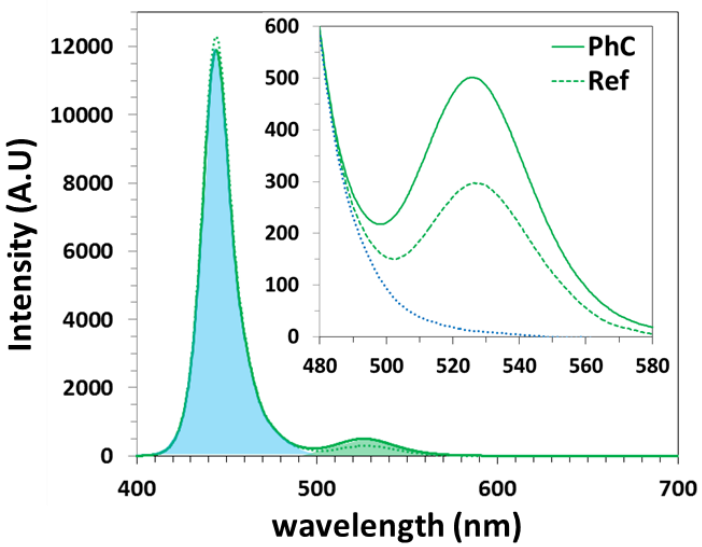

Figure 2-4-14 Measured spectra of single red PhC phosphor plate compared with a reference phosphor plate.

In order to generate white light, I need to convert more blue to red and green, which can be achieved by stacking the phosphor plates in a multiple. Figure 2-4-15 shows the emission spectra for the PhC and reference phosphors composed of the red CQDs when the numbers of stacked phosphor plates are 2 and 6. I intentionally stacked the PhC phosphor plates in a zig-zag manner so that the grating directions of any two adjacent plates are orthogonal to each other to remove the polarization-dependent nature of 1D PhC phosphor structure and thus to make the entire phosphor assembly compatible with the un-polarized excitation condition by a blue LED chip. As the number of phosphor plates increases, the red CQD fluorescence increases whereas the blue LED intensity decreases rapidly. Plotted in the inset are the peak emission intensities of the blue and the red for both the PhC (solid lines) and reference (dashed lines) phosphor stacks, all as functions of the number of phosphor plates. The PhC phosphor stack exhibits stronger red CQD fluorescence and weaker blue LED emission than the reference phosphor stack of the same number of phosphor plates, indicative of higher color conversion efficiency for the PhC phosphor. Roughly speaking, four PhC phosphor plates are competent with six reference phosphor plates. Situations with the green CQD phosphors are similar, as shown in Figure 2-4-16

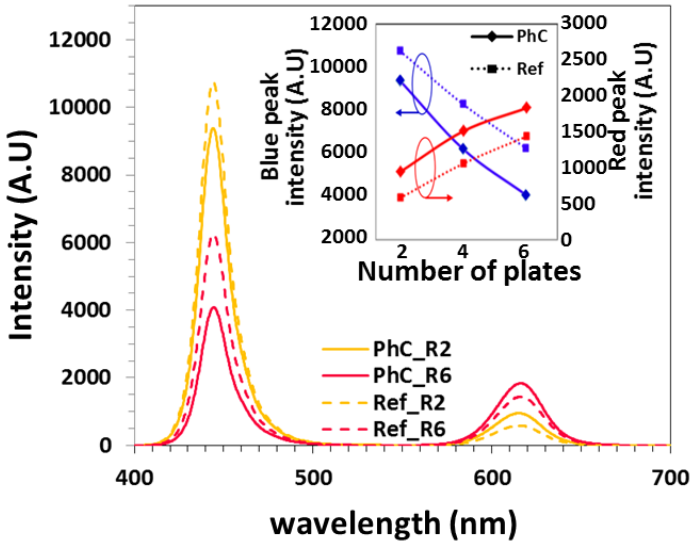

Figure 2-4-15 Measured spectra of multi-stacked red phosphor plates. Inset: blue LED intensity and CQD fluorescence intensity vs. the number of phosphor plates.

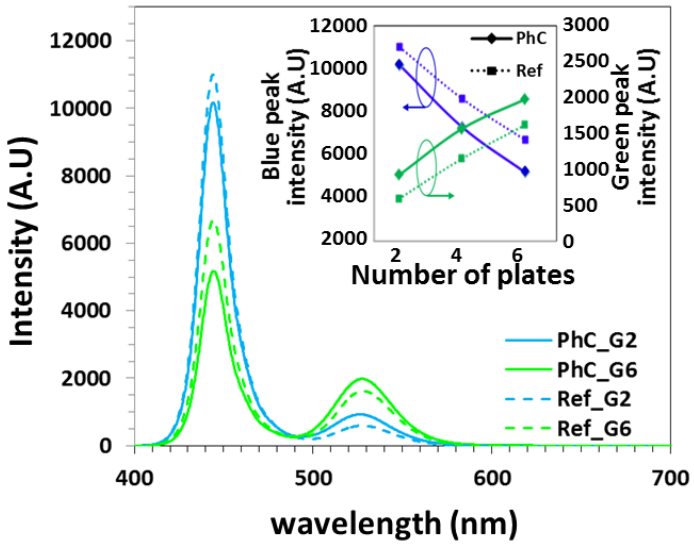

Figure 2-4-16 Measured spectra of multi-stacked red phosphor plates. Inset: blue LED intensity and CQD fluorescence intensity vs. the number of phosphor plates.

2.4.6 White light generation using PhC phosphors

We stacked multiple red and green PhC phosphor plates on a blue LED to generate white light. Two rules were strictly observed when stacking PhC phosphors. First, we stacked the PhC phosphor plates in a zig-zag manner in the grating orientations to remove the polarization-dependent nature of our 1D PhC phosphor structure and thus to make the entire phosphor assembly compatible with the un-polarized excitation condition by a blue LED chip. Second, we stack the red phosphor plates first (right on top of a blue LED chip) and then the green ones (atop the red phosphor plates). Strict observation of this stacking sequence is very important; otherwise green photons emitted from a green phosphor plate would be absorbed by a red phosphor on their way out, deteriorating the overall efficiency of white light generation. Figure 2-4-17 shows schematics of white light generation experiment. For convenience, we denote the stacking configuration by R*m*G*n*, which stands for *m* number of the red phosphor plates and *n* number of the green phosphor plates stacked in sequence. The denotation is prefixed by either PhC or Ref, depending on which kind of phosphor plates are used in the stack. For example, PhC-R3G11 means that three red PhC phosphor plates and eleven green PhC phosphor plates are stacked on a blue LED chip. As for the stacked number of the red PhC phosphor plates, we tried R = 2, 3, and 4 to obtain white light with good chromaticity coordinates. Figure 2-4-18 (a) shows the CIE1931 chromaticity coordinates for the R = 2 and 4 cases. As we increase the number of the green phosphor plates on top of the red phosphor stack, the chromaticity coordinates evolve, but never reach the equal energy point (0.333, 0.333); the chromaticity coordinates are shifted to the blue-green side for R = 2 and to the red side for R =4. When R = 3, however, the evolution of the chromaticity coordinates was in the right

direction as shown in Figure 2-4-18 (b). In fact, we were able to obtain the chromaticity coordinates (0.332, 0.341), which are reasonably close to the equal energy point. The chromaticity coordinates of the data points shown in the figures are summarized in Table 2-4-4.

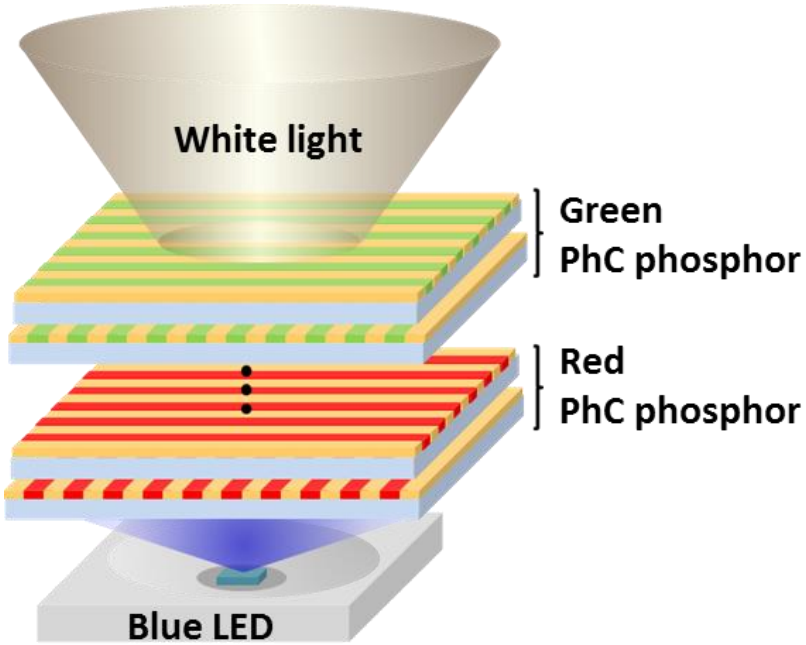

Figure 2-4-17 Schematics of white light generation experiment.

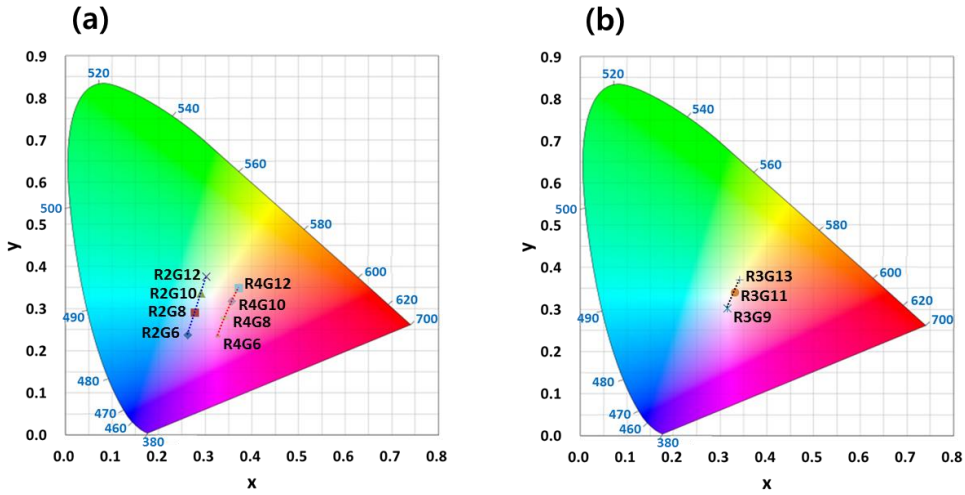

Figure 2-4-18 CIE 1931 chromaticity diagram with the color coordinates marked for the cases of (a) R = 2 and 4, and (b) R = 3. (In all cases, the PhC phosphor was used and the prefix PhC was omitted.)

	x	y
R2G6	0.26	0.24
R2G8	0.28	0.29
R2G10	0.29	0.34
R2G12	0.30	0.38
R3G9	0.32	0.30
R3G11	0.33	0.34
R3G13	0.34	0.37
R4G6	0.32	0.24
R4G8	0.34	0.28
R4G10	0.36	0.32
R4G12	0.37	0.35

Table 2-4-4. CIE1931 chromaticity coordinates (x, y) of the PhC phosphor stack combinations PhC-R*m*G*n* examined.

Figure 2-4-19 shows photographs of (from left to right) Ref-R3G11, PhC-R3G11, and Ref-R5G16, taken directly from the top (upper row) and through the output port of the integrating sphere (lower row). As shown in the middle of Figure 2-4-19, the PhC-R3G11 exhibits decent white light; the corresponding chromaticity coordinates are measured to be (0.332, 0.341) as shown in Figure 2-4-20. In good contrast, the white light source constructed using the reference phosphor plates in the same stacking sequence (*i.e.*, Ref-R3G11) exhibits a quite bluish white hue—the left of Figure 2-4-19; its chromaticity coordinates are (0.216, 0.206), which falls in between the blue and white sectors of the CIE1931 space— Figure 2-4-20. This indicates that blue light from the LED chip is more efficiently converted to red and green with the PhC phosphors than with the reference phosphors. In order to construct a white light source with the color coordinates similar to those of PhC-R3G11 using the reference phosphor plates only, we had to employ substantially increased numbers of phosphor plates: Ref-R5G16. Emission images of the device are shown in the right of Figure 2-4-19 while its chromaticity coordinates came out to be (0.331, 0.336)— Figure 2-4-20. The correlated color temperatures of the two decent white light sources, PhC-R3G11 and Ref-R5G16, are found to be ~5500 K, as shown in Figure 2-4-21. Figure 2-4-22 compares the emission spectra of the two white light sources, PhC-R3G11 and Ref-R5G16. Although PhC-R3G11 contains ~33% less CQDs than Ref-R5G16, the former exhibits 8% higher integrated intensity than the latter, thanks to an enhanced absorption (thus a higher color conversion efficiency) enabled by the structural engineering of phosphor materials.

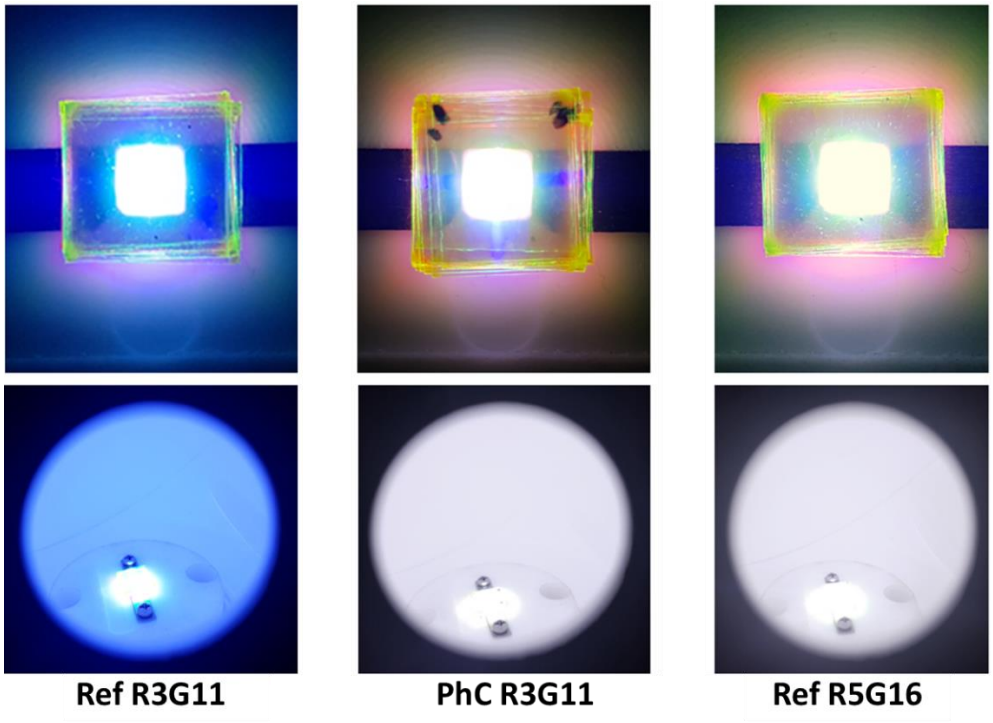

Figure 2-4-19 Photograph images of top view of the sample (upper) and inside the integrating sphere (lower) for Ref R3G11(left), PhC R3G11(middle), Ref R5G16(right).

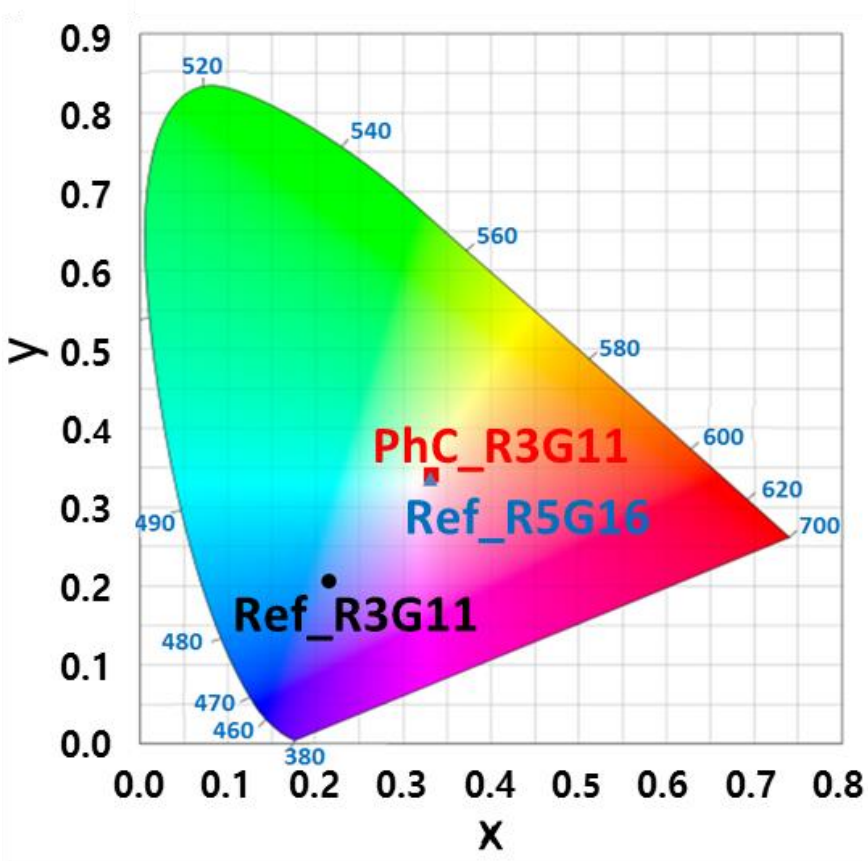

Figure 2-4-20 CIE chromaticity diagram with results obtained from Ref R3G11, PhC R3G11 and Ref R5G16.

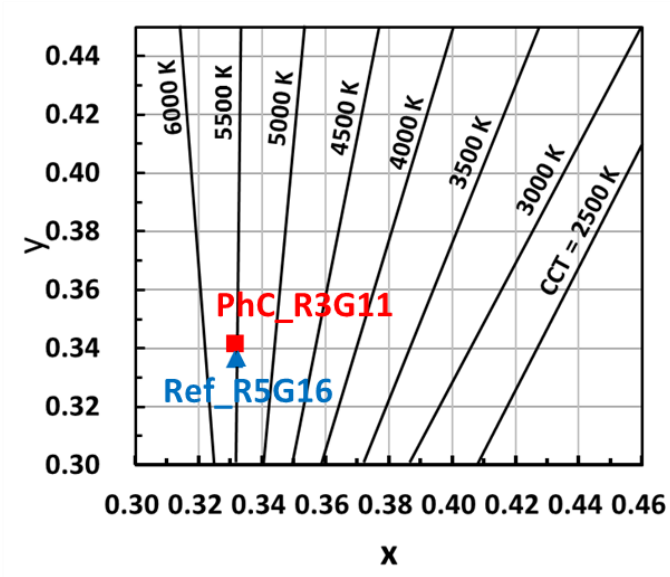

Figure 2-4-21 Close up of white region of CIE chromaticity diagram with results obtained from PhC R3G11 and Ref R5G16 for evaluating CCT.

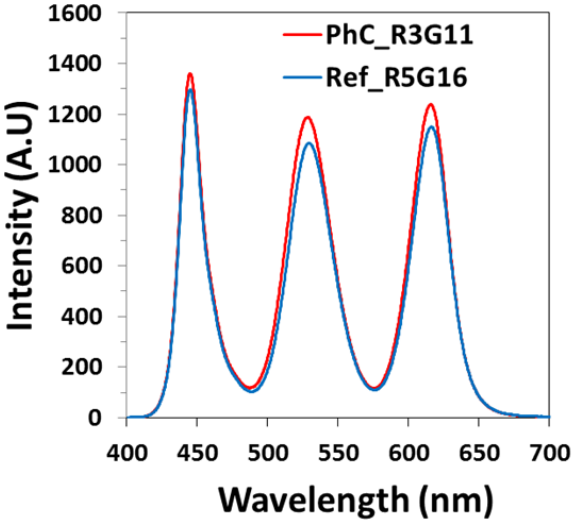

Figure 2-4-22 Emission spectra of PhC R3G11 and Ref R5G16.

2.5 Summary

An efficient white light source platform using structurally engineered phosphors was demonstrated. PhC phosphors composed of red and green colloidal quantum dots were stacked on a blue LED chip. With the photonic band-edge modes in resonance with the energy of blue excitation photons, more white light was generated out of a significantly less amount of phosphor materials than the reference device.

Finite-difference time-domain (FDTD) simulations were performed to predict the performance characteristics and to find the optimum structures of the PhC phosphors. I designed the red and green PhC phosphors to match their band-edge modes with excitation photon energy from the blue LED chip. The excitation resonance improves the interaction between the excitation photons from the blue LED chip and CQDs, resulting in enhanced absorption of excitation photons by CQDs and thus enhanced emission.

I fabricated the corresponding lateral 1D PhC phosphor structure patterned by LHL method, and CQDs were spin-coated thereon. The prepared red and green PhC phosphors were improved in fluorescence intensity by ~5.5 times and ~3.1 times, respectively, compare with the reference phosphors.

By progressively stacking the PhC phosphor plates on a blue LED chip, the blue, green, and red emission intensities can be tightly controlled to obtain white light with the desired properties. The chromaticity coordinates, (0.332, 0.341), and correlated color temperature, 5500 K, are obtained from a stack of 3 red and 11 green PhC phosphor plates; in contrast, a stack of 5 red and 16 green reference

phosphor plates are required to generate a similar white light. Overall, the PhC phosphors produce 8% higher total emission intensity out of 33% less amount of CQDs than the reference phosphors, thanks to a higher color conversion efficiency enabled by the structural engineering of phosphor materials.

This result proves that our PhC phosphor platform is not just a concept but also a viable technology enabled by structural engineering of any phosphor materials, therefore a paradigm-shifting way of developing next-generation high efficiency phosphors.

References

[1] E. F. Schubert and J. K. Kim, “Solid-state light sources getting smart,” Science **308**, 1274 (2005).

[2] M. R. Krames, O. B. Shchekin, R. Mueller-Mach, G. O. Mueller, L. Zhou, G. Harbers and M. G. Craford, “Status and Future of High-Power Light-Emitting Diodes for Solid-State Lighting ,” IEEE J. Display Technol. **3**, 160 (2007).

[3] R.-J. Xie, N. Hirosaki and T. Takeda, “Wide Color Gamut Backlight for Liquid Crystal Displays Using Three-Band Phosphor-Converted White Light-Emitting Diodes,” Appl. Phys. Express **2**, 022401 (2009).

[4] C. J. Humphreys, “Solid-State Lighting,” MRS Bull. **33**, 459 (2008).

[5] A. Laubsch, M. Sabathil, J. Baur, M. Peter and B. Hahn, “High-Power and High-Efficiency InGaN-Based Light Emitters,” IEEE Trans. Electron Devices **57**, 79 (2010).

[6] K. J. Chen, H. V. Han, B. C. Lin, H. C. Chen, M. H. Shih, S. H. Chien, K. Y. Wang, H. H. Tsai, P. Yu, P. T. Lee, C. C. Lin and H. C. Kuo, “Improving the Angular Color Uniformity of Hybrid Phosphor Structures in White Light-Emitting Diodes,” IEEE Electron Device Lett. **34**, 1280 (2013).

[7] J. M. Caruge, J. E. Halpert, V. Wood, V. Bulovic and M. G. Bawendi, “Colloidal quantum-dot light-emitting diodes with metal-oxide charge transport layers,” Nat. Photonics **2**, 247 (2008).

[8] E. F. Schubert, *Light-Emitting Diodes* (Cambridge University Press 2008).

[9] K. Bando, K. Sakano, Y. Noguchi and Y. Shimizu, “Development of High-bright and Pure-white LED Lamps,” J. Light Vis. Env. **22**, 2 (1998).

[10] C. Feldmann, T. Jüstel, C. R. Ronda and P. J. Schmidt, “Inorganic Luminescent Materials: 100 Years of Research and Application,” Adv. Func. Mater. **13**, 511 (2003).

[11] S. Pimputkar, J. S. Speck, S. P. DenBaars and S. Nakamura, “Prospects for LED lighting,” Nat. Photonics **3**, 180 (2009).

[12] P. Pust, V. Weiler, C. Hecht, A. Tücks, A. S. Wochnik, A.-K. Henß, D. Wiechert, C. Scheu, P. J. Schmidt and W. Schnick, “Narrow-band red-emitting $Sr[LiAl_3N_4]:Eu^{2+}$ as a next-generation LED-phosphor material,” Nat. Mater. **13**, 891 (2014).

[13] H. Daicho, T. Iwasaki, K. Enomoto, Y. Sasaki, Y. Maeno, Y. Shinomiya, S. Aoyagi, E. Nishibori, M. Sakata, H. Sawa, S. Matsuishi and H. Hosono, “A novel phosphor for glareless white light-emitting diodes,” Nat. Commun. **3**, 1132 (2012).

[14] W. B. Im, N. George, J. Kurzman, S. Brinkley, A. Mikhailovsky, J. Hu, B. F. Chmelka, S. P. DenBaars and R. Seshadri, “Efficient and Color-Tunable Oxyfluoride Solid Solution Phosphors for Solid-State White Lighting,” Adv. Mater. **23**, 2300 (2011).

[15] C.-Y. Sun, X.-L. Wang, X. Zhang, C. Qin, P. Li, Z.-M. Su, D.-X. Zhu, G. -G. Shan, K. -Z. Shao, H. Wu and J. Li, “Efficient and tunable white-light emission of metal–organic frameworks by iridium-complex encapsulation,” Nat. Commun. **4**, 2717 (2013).

[16] K. Min, Y.-K. Choi and H. Jeon, “Model calculations for enhanced fluorescence in photonic crystal phosphor,” Opt. Express **20**, 2452 (2012).

[17] K. Min, S. Choi, Y. Choi and H. Jeon, “Enhanced fluorescence from CdSe/ZnS quantum dot nanophosphors embedded in a one-dimensional photonic crystal

backbone structure," Nanoscale **6**, 14531 (2014).

[18] K. Min, H. Jung, Y. Park, K.-S. Cho, Y.-G. Roh, S. Hwang and H. Jeon, "A colloidal quantum dot photonic crystal phosphor: nanostructural engineering of the phosphor for enhanced color conversion," Nanoscale **9**, 8703 (2017).

[19] J. P. Dowling, M. Scalora, M. J. Bloemer and C. M. Bowden, "The photonic band edge laser: A new approach to gain enhancement," J. Appl. Phys. **75**, 1896 (1994).

[20] John D. Joannopoulos, Robert D. Meade, and Joshua N. Winn, *Photonic crystals: Molding the flow of light* (Princeton University Press 2008).

[21] T. Baba, "Slow light in photonic crystals," Nat. Photonics **2**, 465 (2008).

[22] C. M. Johnson, P. J. Reece and G. J. Conibeer, "Slow-light-enhanced upconversion for photovoltaic applications in one-dimensional photonic crystals," Opt. Lett. **36**, 3990 (2011).

[23] http://www.lumerical.com

[24] C. Kittel, *Introduction to Solid State Physics, 8th ed.* (Wiley 2004).

[25] J. D. Jackson, *Classical Electrodynamics, 3rd ed.* (Wiley 1998).

[26] E. D. Palik, *Handbook of Optical Constants of Solids* (Elsevier **1998)**.

[27] S. R. J. Brueck, "Optical and interferometric lithography-Nanotechnology enablers," Proceedings of the IEEE **93**, 1704 (2005).

[28] T. C. Hennessy, *Lithograpy: Principles, Processes and Materials* (Nova Science Publishers 2011).

[29] W. Hinsberg, F. A. Houle, J. Hoffnagle, M. Sanchez, G. Wallraff, M. Morrison and S. Frank, "Deep-ultraviolet interferometric lithography as a tool for

assessment of chemically amplified photoresist performance," J. Vac. Sci. Technol. B **16**, 3689 (1998).

[30] D.-H. Kim, C.-O Cho, Y.-G. Roh, H. Jeon, Y. S. Park, J. Cho, J. S. Im, C. Sone, Y. Park, W. J. Choi and Q-H. Park, "Enhanced light extraction from GaN-based light-emitting diodes with holographically generated two-dimensional photonic crystal patterns," Appl. Phys. Lett. **87**, 203508 (2005).

[31] D.-Y. Kim, S. K. Tripathy, L. Li, and J. Kumar, "Laser-induced holographic surface relief gratings on nonlinear optical polymer films," Appl. Phys. Lett. **66**, 1166–1168 (1995).

[32] J. H. Moon, S.-M. Yang, D. J. Pine, and W.-S. Chang, "Multiple-exposure holographic lithography with phase shift," Appl. Phys. Lett. **85**, 4184–4186 (2004).

[33] K. Min, "Photonic crystal Phosphors", (Seoul national university graduate school 2015)

[34] B. E. E. Kastenmeier, P. J. Matsuo, and G. S. Oehrlein, "High selective etching of silicon nitride over silicon and silicon dioxide," J. Vac. Sci. Technol. A **17**, 3179–3184 (1999).

[35] S. Abe, J. J. Joos, L. I. D. J. Martin, Z. Hens and P. F. Smet, "Hybrid remote quantum dot/powder phosphor designs for display backlights," Light Sci. Appl. **6**, e16271 (2017).

[36] J. Lim, S. Jun, E. Jang, H. Baik, H. Kim and J. Cho, "Preparation of Highly Luminescent Nanocrystals and Their Application to Light-Emitting Diodes," Adv. Mater. **19**, 1927 (2007).

[37] K.-S. Cho, E. K. Lee, W.-J. Joo, E. Jang, T.-H. Kim, S. J. Lee, S.-J. Kwon, J. Y.

Han, B.-K. Kim, B. L. Choi and J. M. Kim, “High-performance crosslinked colloidal quantum-dot light-emitting diodes,” Nat. Photonics **3**, 341 (2009).

[38] T.-H. Kim, K.-S. Cho, E. K. Lee, S. J. Lee, J. Chae, J.W. Kim, D. H. Kim, J.-Y. Kwon, G. Amaratunga, S.Y. Lee, B. L. Choi, Y. Kuk, J. M. Kim and K. Kim, “Full-colour quantum dot displays fabricated by transfer printing,” Nat. Photonics **5**, 176 (2011).

Chapter 3

2D Photonic Crystal Phosphors

3.1 Introduction

I explored the characteristics of the lateral 1D PhC phosphors, and using this I demonstrated an efficient white light generating method in chapter 2. The dependence of the lateral 1D PhC phosphors on the polarization direction of excitation source was also examined. Electric fields are naturally perpendicular to the direction of propagation. Thus, if an external excitation photon incident perpendicularly to the surface of a 1D PhC phosphor, the direction of the electric field should be parallel to the surface. In addition, the direction of wave vectors of the PBE mode of the lateral 1D PhC is parallel to periodicity, so the direction of the electric field of PBE mode should be parallel to grating direction or perpendicular to the surface. In order to satisfy both conditions, the polarization direction of the excitation photon must be parallel to grating direction. To remove this polarization-dependent nature of the lateral 1D PhC phosphor structure and thus to make the entire phosphor assembly compatible with the un-polarized excitation condition by a blue LED chip, I intentionally stacked the PhC phosphor plates in a zig-zag manner so that the grating directions of any two adjacent plates are orthogonal to each other [1]. On the other hand, 2D PhC phosphors have rotational symmetry and are expected to be independent on the polarization direction of the excitation source. Figure 3-1-1 shows the schematics of the lateral 1D PhC phosphor and the 2D PhC phosphor with the polarization direction that can be resonated with PBE mode.

In 2D PhC phosphors, lattice constants in the x and y directions can be designed differently. In this thesis, 2D PhC phosphor structures with different lattice constant in x and y directions are called as asymmetric 2D PhC phosphors. As shown in the Figure 3-1-2, the asymmetric 2D PhC phosphor has a photonic band structure different from that of the symmetric 2D PhC phosphor, and thus its performance characteristics are also different from those of the symmetric 2D PhC phosphor.

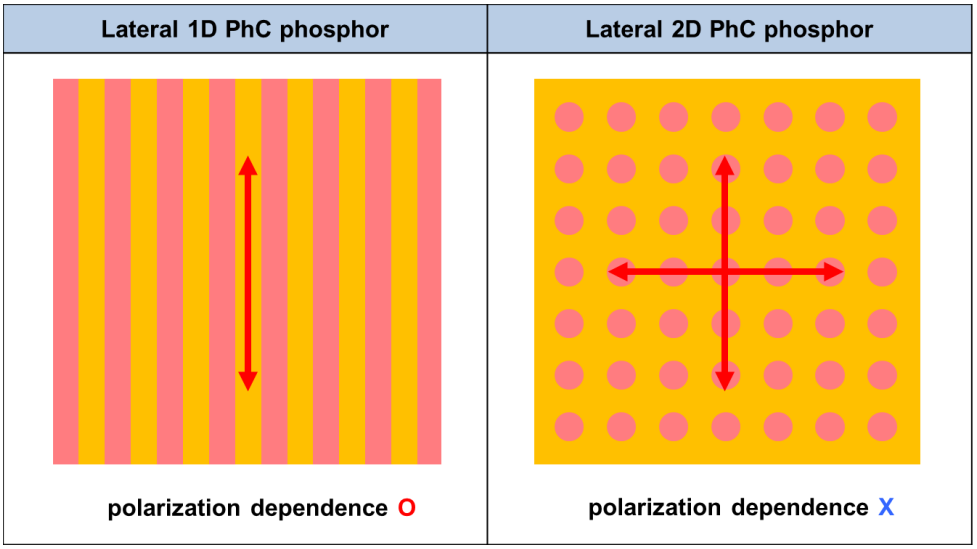

Figure 3-1-1 Schematics of the lateral 1D PhC phosphor and the 2D PhC phosphor with the polarization direction that can be resonated with PBE mode.

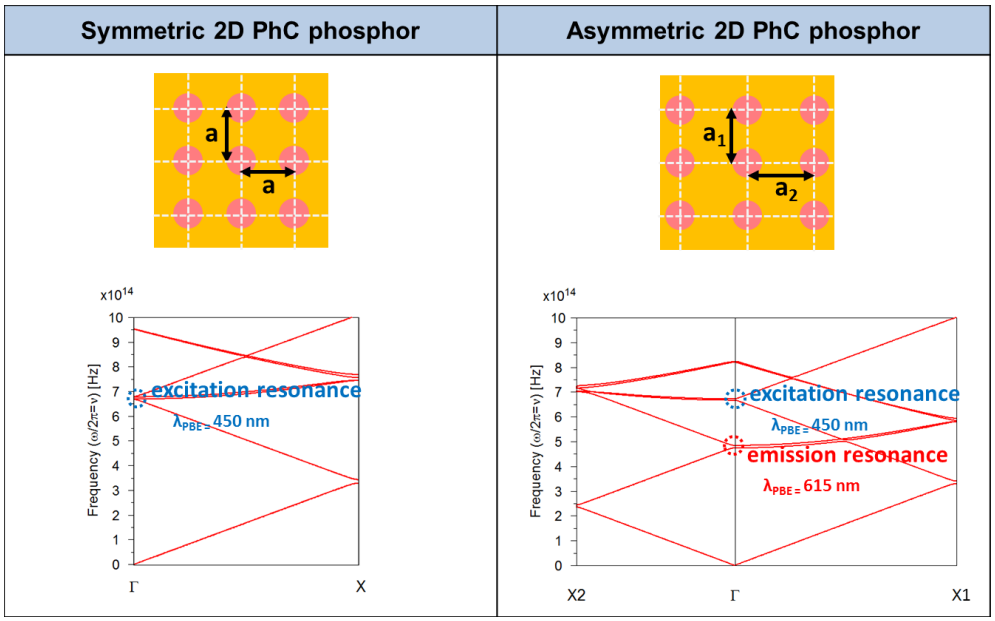

Figure 3-1-2 Comparison of photonic band structure of the symmetric and the asymmetric 2D PhC.

3.2 Device design and Fabrication

3.2.1 Photonic band structure of 2D PhC by plain wave expansion method

I calculated the photonic band structures of 2D square lattice PhCs using plain wave expansion (PWE) method [2,3]. As mentioned in Chapter1, PWE method is very useful and powerful technique for investigation of the photonic band structures of PhCs. Especially, in 2D simulations, the PWE method quickly gets modal solutions that describe the photonic band and field profile. However, it is difficult to use the PWE method in 3D calculations where thickness of PhC slabs, substrates, etc. should be considered. Therefore, I used the modified dielectric constants method to convert the 3D structure into a corresponding 2D structure [4,5], as schematically shown in Figure 3-2-1. First I estimate the n_{eff} and Γ using Transfer-matrix (TM) method [6]**.** Where n_{eff} is the effective refractive index reflecting the 3D structure and Γ is a confinment factor indicating how much the electric field overlaps the PhC slab. Second, the modified dielectric constants of hole and background, ε_a and ε_b are obtained by the following two equations.

$$n_{eff}^2 = f\varepsilon_a + (1-f)\varepsilon_b \cdots (1)$$

where f is the filling factor, which is the ratio of the hole area to the total area.

$$\varepsilon_a - \varepsilon_b = \Gamma(\varepsilon_{hole} - \varepsilon_{bg}) \cdots (2)$$

Figure 3-2-2 shows the electric field intensity distribution of the 2D square lattice PhC phosphor consisting of glass, Si_3N_4/CQD and air obtained by TM method, and the refractive indices of each layer. The TM method yielded Γ and n_{eff} of 74% and 1.72, respectively. Using the refractive indices 2.04 and 1.82 for Si_3N_4 and CQDs in

calculation, I obtained modified dielectric constants, ε_a and ε_b value of 2.45 and 3.08, respectively by equation (1) and (2).

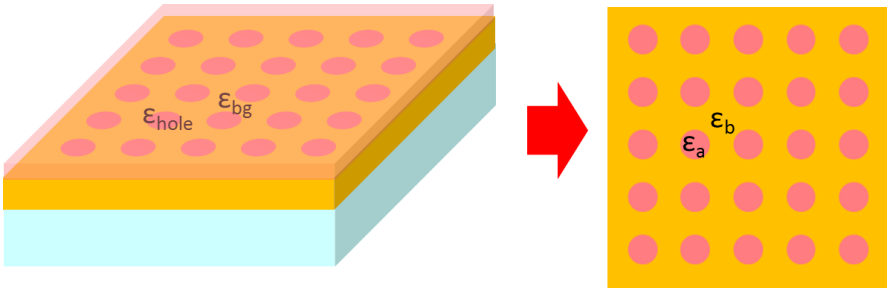

Figure 3-2-1 Schematic description of modified dielectric method.

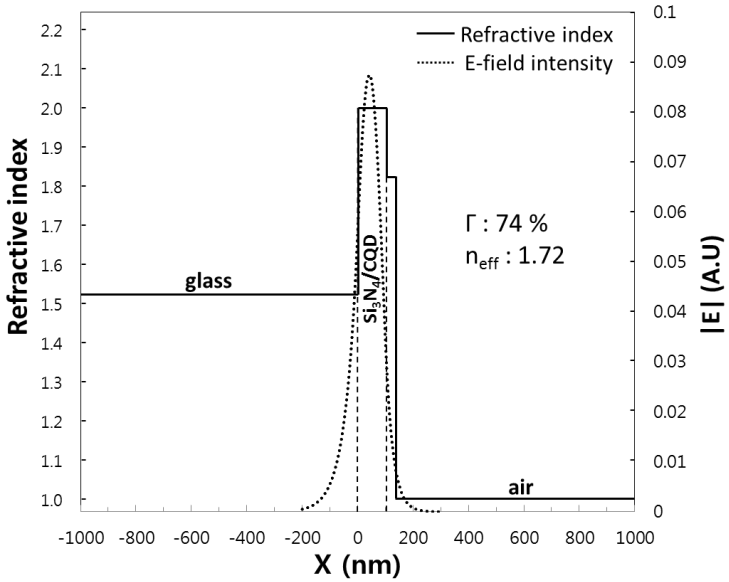

Figure 3-2-2 Electric field intensity distribution of the 2D square lattice PhC phosphor consisting of glass, Si_3N_4/CQD and air obtained by TMM method, and the refractive indices of each layer.

Finally, photonic band structure of 2D square lattice PhC, where lattice constant a = 280nm, r = 0.25a (filling factor ~20%), was calculated using PWE method and shown in Figure 3-2-3.

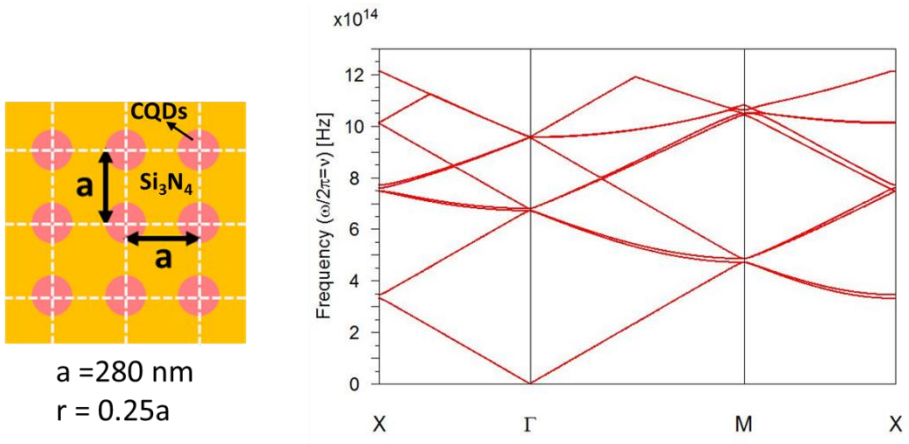

Figure 3-2-3 Photonic band structure of the 2D square lattice PhC phosphor.

There are three symmetric points of Γ-, X- and M-point in the 2D square lattice PhC. Figure 3-2-4 shows the Brillouin zone of the 2D square lattice PhC and the direction of the wave vector of each symmetric point. At Γ point, $k_{//} = 0$, where k is a wave vector parallel to the x-y plane. On the other hand, $k_{//} \neq 0$ at other symmetric points. When the excitation photon is incident perpendicular to the x-y plane, it can be coupled with Γ point PBE modes, but not with the others. Therefore, I used the Γ point PBE modes in generating 2D PhC phosphors. The wavelength of the lowest order Γ point PBE modes is ~ 450 nm, which is suitable for resonance with a blue excitation photon.

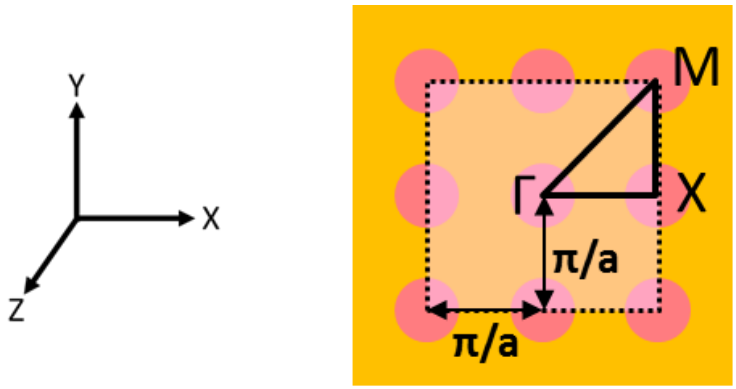

Figure 3-2-4 Brillouin zone of the 2D square lattice PhC.

So far, I have examined the photonic band structure of the 2D square lattice PhC with the same lattice constant in x and y directions. In this thesis, I called the 2D square lattice PhC as the symmetric 2D PhC, as compared to the asymmetric 2D PhC described in the following. Next, I calculated the photonic band structure of the asymmetric 2D PhC, which has different lattice constant in x and y directions. Figure 3-2-5 shows the photonic band structure of asymmetric 2D PhC with a_1 = 280 nm, a_2 = 400 nm. As shown in Figure 3-2-3, four Γ point band edges are approximately at the same position (wavelength is ~ 450 nm) in the 2D symmetric PhC. On the other hand, four Γ point band edges are separated from each other by two (wavelengths are ~ 450 nm, ~610 nm) in the 2D asymmetric PhC. I expected that the upper PBE modes (wavelength ~450nm) would resonate with the excitation photons and the lower PBE modes would resonate with the emission photons (from CQDs), resulting in higher enhancement factor.

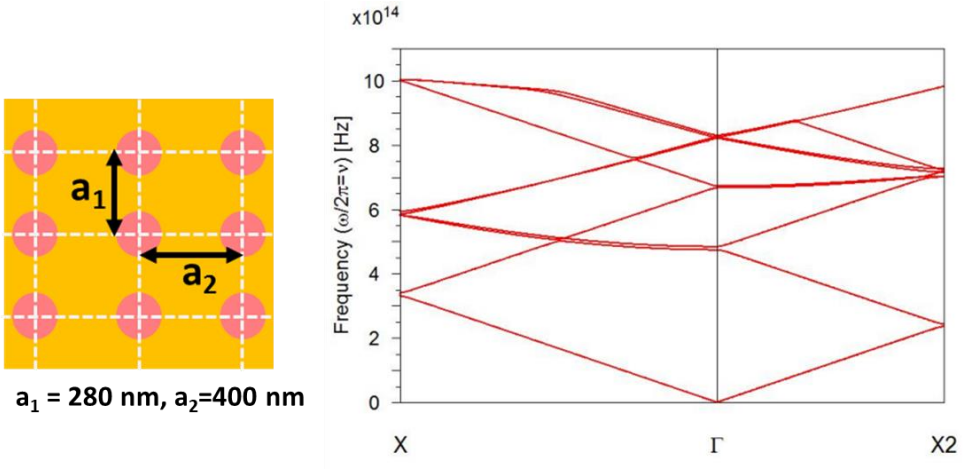

Figure 3-2-5 Photonic band structure of the 2D asymmetric PhC.

3.2.2 Photonic band structure and absorbance spectra of 2D PhC by FDTD

In the previous section, the photonic band structures of 2D PhCs were calculated using modified dielectric constant method and PWE method. In this section, to confirm the validity of the method used in the previous section, photonic band structures reflecting the 3D structure were obtained using 3D FDTD method [7]. Figure 3-2-6 shows the photonic band structure of the 2D PhC using 3D FDTD method, which is almost identical to photonic band structure using PWE method, shown in Figure 3-2-3. However, 3D FDTD method took a few days to calculate, while the PWE method took only 1 minute. So I used the PWE method to calculate photonic band structures except in special cases.

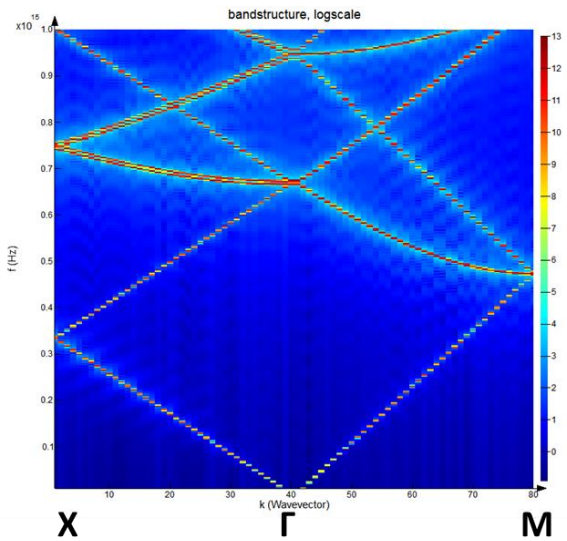

Figure 3-2-6 Photonic band structure of the 2D PhC phosphor using 3D FDTD method.

Next, I obtained absorbance spectra of symmetric 2D PhC phosphors using FDTD method. I described the polarization dependence of lateral 1D PhC phosphors in Chapter 1. On the other hand, 2D symmetric PhC phosphors have rotational symmetry and are expected to be independent of the polarization direction of the excitation source. I compared absorbance spectra of the symmetric 2D PhC phosphor with excitation source polarized at 0˚, 45˚and 90˚, as can be seen in Table 3-2-1. It exhibits the same absorbance spectrum regardless of the polarization direction of excitation source, and is a unique property of the symmetric 2D PhC phosphors distinguished from the lateral 1D PhC phosphors. This polarization independence property of the symmetric 2D PhC phosphors is a great help in applying to real light emitting devices.

Pol. angle	0 ˚	45 ˚	90 ˚
excitation source polarization	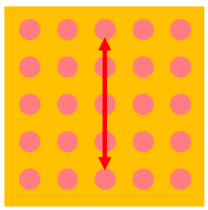	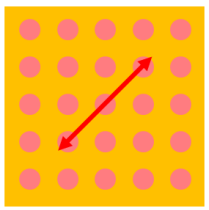	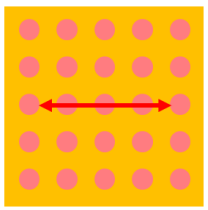
Absorbance spectra	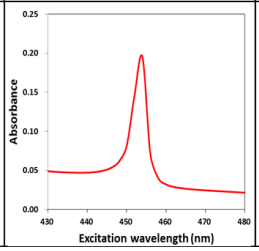	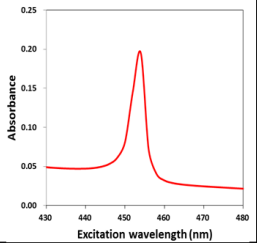	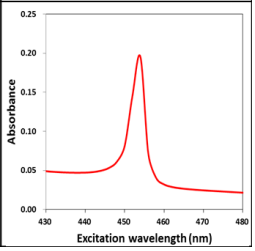

Table 3-2-1 Comparison of absorbance spectra of the symmetric 2D PhC phosphor with excitation source polarized at 0˚, 45˚and 90˚

Next, I also calculated absorbance spectra of the 2D asymmetric PhC phosphors. Table 3-2-2 shows absorbance spectra of the 2D asymmetric PhC phosphors when excitation source was polarized at 0˚, 45˚and 90˚.

Asymmetric 2D PhC phosphors exhibit polarization dependence in absorbance spectra due to different lattice constants in x and y directions. As expected from the calculation of the photonic band structure, absorbance peaks due to the PBE effect is observed at two excitation wavelengths of ~450 nm and ~610 nm.

Pol. angle	0 °	45 °	90 °
excitation source polarization	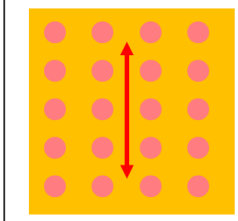	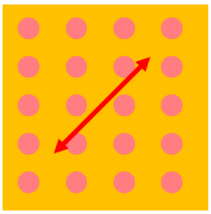	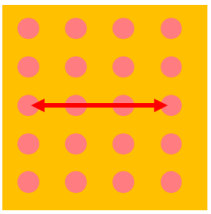
Absorbance spectra	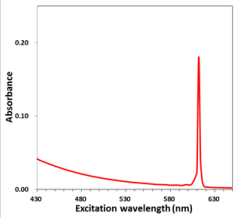	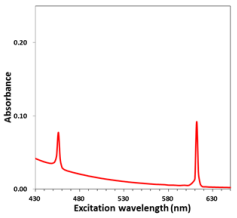	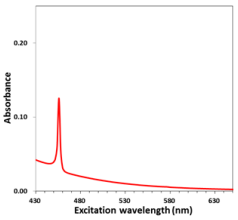

Table 3-2-2 Comparison of absorbance spectra of the asymmetric 2D PhC phosphor with excitation source polarized at 0˚, 45˚and 90˚

3.2.3 Device fabrication

2D PhC samples were fabricated with the same process steps as the 1D lateral PhC phosphor as shown in the Figure 2-3-2. 2D PR pattern was formed by the Laser holographic lithography (LHL) method [8,9] on the Si_3N_4 deposited glass substrate, and PR pattern was subsequently transferred to the Si_3N_4 layer by reactive-ion etching (RIE). Finally, red CQDs were spin-coated on top of the 2D Si_3N_4 pattern. See section 2.3.1 for more details. Unlike the case of 1D lateral PhC phosphors, one additional exposure was performed on 90°-rotated samples in the LHL process [10]. For comparison, CQDs were spin-coated on a flat glass substrate to produce a reference phosphor. Figure 3-2-3 shows scanning electron microscope (SEM) images of the symmetric 2D PhC phosphor and the asymmetric 2D PhC phosphor after LHL process. I fabricated three kinds of sample; the 280 nm x 280 nm sample designed to cause excitation resonance with excitation source, the 400 nm x 400 nm sample designed to cause emission resonance with photons emitted from the red CQDs and 280 nm x 400 nm sample designed for both excitation resonance and emission resonance.

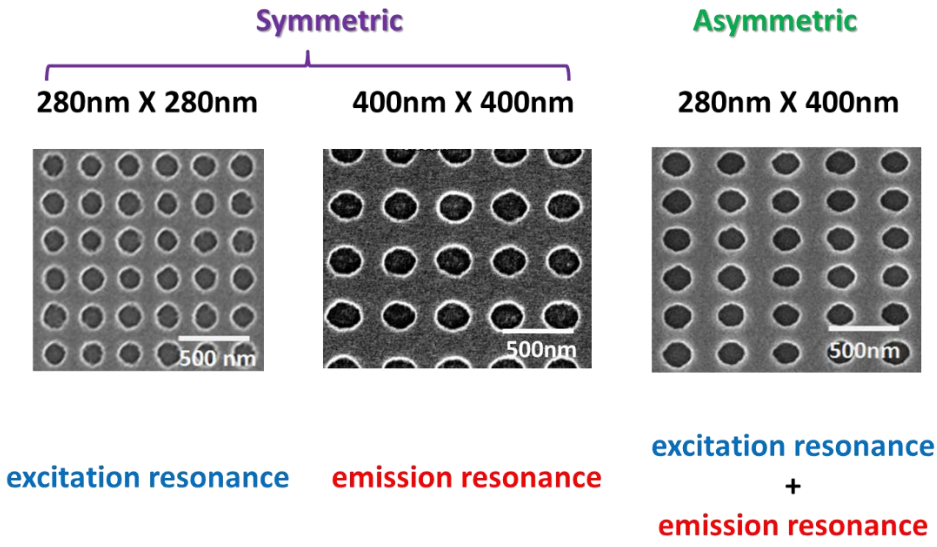

Figure 3-2-7 SEM images of the 280 nm x 280 nm sample(left), 400 nm x 400 nm sample (middle) and the 280 nm x 400 nm sample (right) after LHL process.

3.3 Measurement and Analyses

3.3.1 Transmittance spectra measurement

To investigate properties of the fabricated 2D PhC phosphors, we performed transmittance spectra measurement. The simplest way to measure the PBE wavelength of PhC phosphors is to measure transmittance. As shown in the simulation in the previous section, the absorbance at the PBE wavelength has the local maximum value, which causes the transmittance to be local minimum at the PBE wavelength. Figure 3-3-1 shows the transmittance spectrum of the 280 nm x 280 nm sample. The transmittance dip, corresponding to the absorbance peak in the absorbance spectra, was observed at 445 nm. There is a slight difference in the PBE wavelength from the FDTD simulation. This is because the structure used in the simulation and the actually fabricated structure are different in hole size, surface morphology, and so on. Figure 3-3-2 shows the transmittance spectrum of the 400 nm x 400 nm sample. The transmittance dip was observed at 610 nm, which is in good agreement with the FDTD simulation. I also measured the transmittance of the 280 nm x 400 nm sample. Figure 3-3-3 shows the transmittance spectrum of the asymmetric 2D PhC phosphor with a_1 = 280 nm, a_2 = 400 nm. Using unpolarized white light for transmittance measurements, two transmittance dips were observed as expected in the simulation.

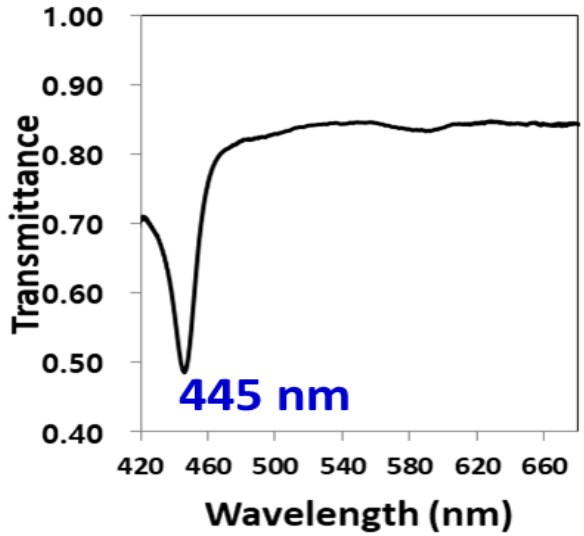

Figure 3-3-1 Transmittance spectrum of the 280 nm x 280 nm sample.

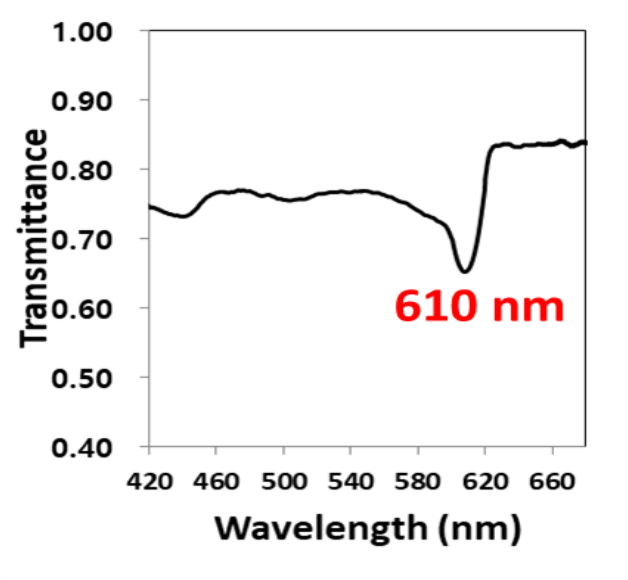

Figure 3-3-2 Transmittance spectrum of the 400 nm x 400 nm sample.

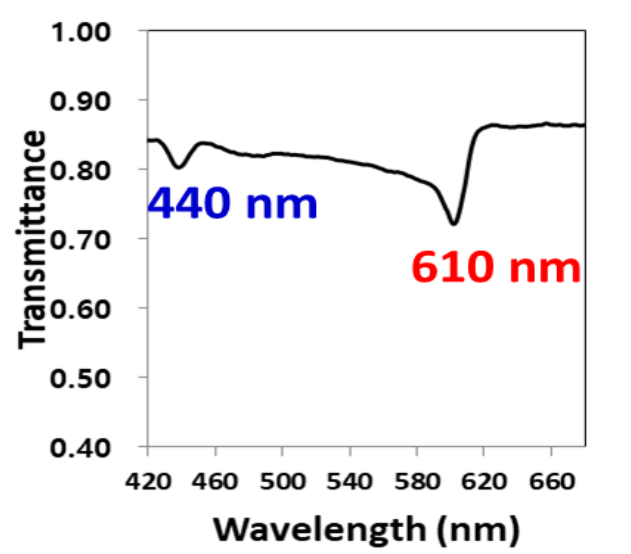

Figure 3-3-3 Transmittance spectrum of the 280 nm x 400 nm sample.

3.3.2 Photoluminescence measurement and enhancement factor

To investigate enhancement factors of 2D PhC phosphors, we performed photoluminescence (PL) excitation experiments using the same setup used in lateral1D PhC phosphors in section 2-4-2. Table 3-3-1 shows the PL intensity spectra of the 280 nm x 280 nm sample and the reference phosphor and the PL enhancement factor plotted as a function of excitation wavelength, which is obtained by taking the PL intensity ratio between the PhC phosphor and the reference phosphor at a given excitation wavelength when excitation source was polarized at 0˚ and 90˚. It exhibits almost the same enhancement factor of ~6.0 regardless of the polarization of excitation source, and is a unique property of the symmetric 2D PhC phosphor distinguished from the lateral 1D PhC phosphor. This polarization independence property of the symmetric 2D PhC phosphor is a great help in applying to white LEDs and other applications. The PL intensity spectra and the PL enhancement factor of the 400 nm x 400 nm sample were also obtained by the same procedure, and Table 3-3-2 shows the result. The enhancement factor was ~3 in all excitation wavelength regions both when the excitation source was 0˚ polarization and 90˚polarization. It means that only emission resonance occurs.

The PL intensity spectra and the PL enhancement factor of the asymmetric 2D PhC phosphor, 280 nm x 400 nm sample, were also obtained by the same procedure, and the results are shown in the Table 3-3-3. When the excitation source was 0˚ polarization, the enhancement factor was ~3 in all excitation wavelength regions. It means that only emission resonance with photon emitted from CQDs occurs. On the other hand, when the excitation source was 90˚ polarization, the enhancement peak with a value of ~12 was observed at an excitation wavelength of ~ 445 nm, and the enhancement factor converged to about 3 as the excitation

wavelength goes away from the excitation resonance. It means that the upper PBE modes (wavelength ≈ 445 nm) of the asymmetric PhC phosphor were resonated with the excitation photons and the lower PBE modes (wavelength ≈ 610nm) were resonated with the photons emitted from CQDs, result in the higher enhancement factor of ~12.

	Excitation source Polarization	Integrated PL intensity	PL enhancement factor
0 °	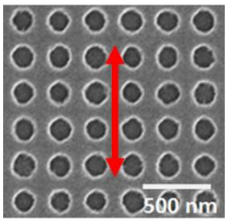	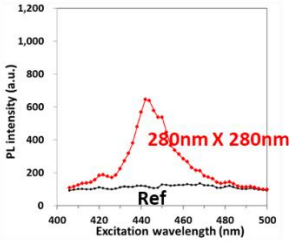	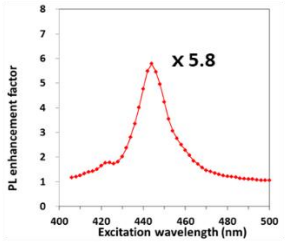
90 °	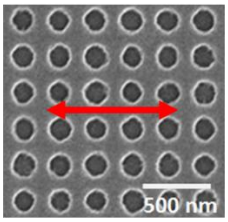	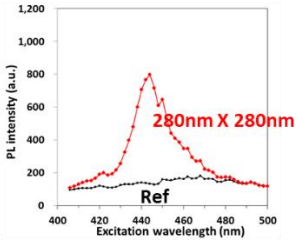	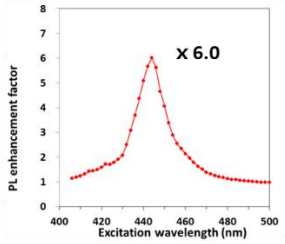

Table 3-3-1 PL intensity spectra and PL enhancement factor of the 280 nm x 280 nm sample when excitation source was polarized at 0˚(upper) and 90˚(lower)

	Excitation source Polarization	Integrated PL intensity	PL enhancement factor
0 °	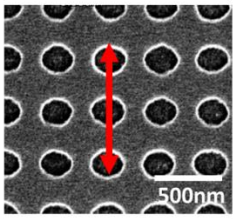	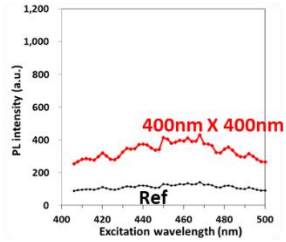	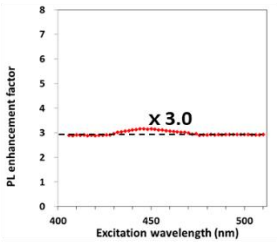
90 °	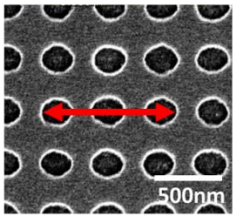	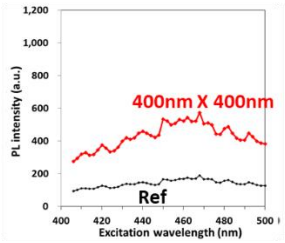	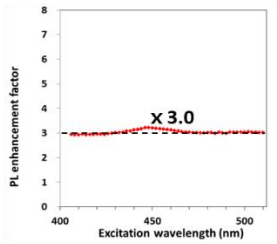

Table 3-3-2 PL intensity spectra and PL enhancement factor of the 400 nm x 400 nm sample when excitation source was polarized at 0˚(upper) and 90˚(lower)

	Excitation source Polarization	Integrated PL intensity	PL enhancement factor
0 °	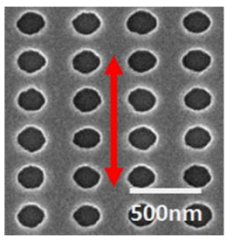	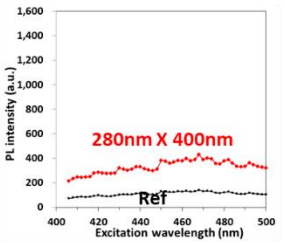	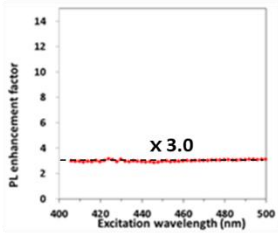
90 °	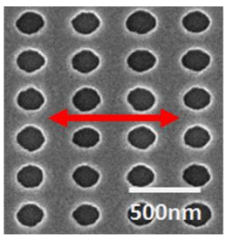	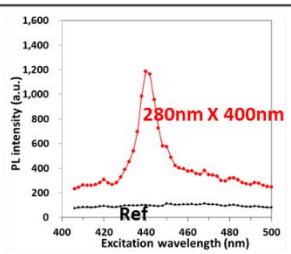	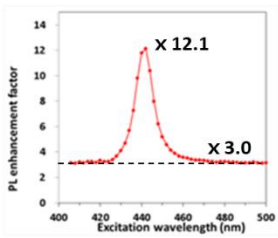

Table 3-3-3 PL intensity spectra and PL enhancement factor of the 280 nm x 400 nm sample when excitation source was polarized at 0˚(upper) and 90˚(lower)

Table 3-3-4 shows the PL spectra of the 280 nm x 280 nm sample, the 400 nm x 400 nm sample and the 280 nm x 400 nm sample at two different excitation wavelength. It is noteworthy that when excitation resonance occurs, only the fluorescence intensity was increased without changing the shape of the spectrum. On the other hand, when the emission resonance occurs, the spectral shape changed.

	Excitation source Polarization	Integrated PL intensity	PL spectra	
			Resonance	Off-resonance
280X280	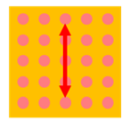	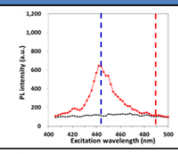	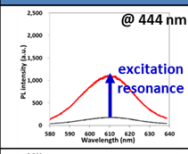	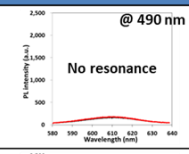
	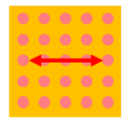	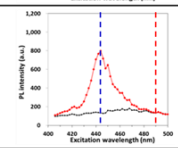	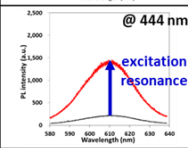	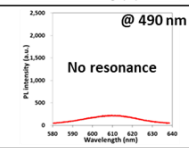
400X400	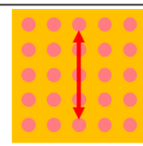	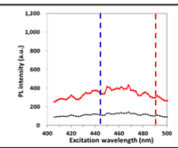	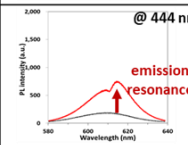	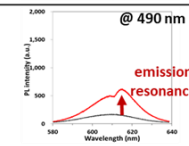
	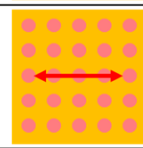	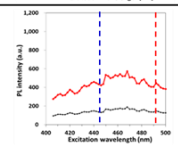	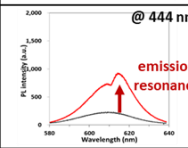	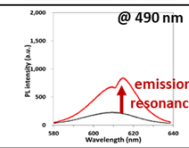
280X400	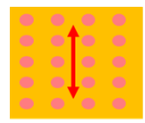	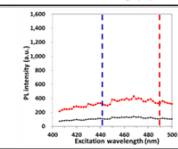	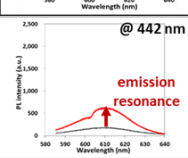	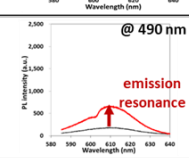
	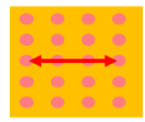	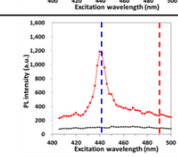	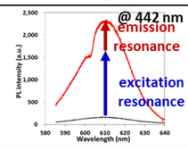	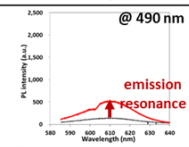

Table 3-3-4 PL spectra of the 280 nm x 280 nm sample, the 400 nm x 400 nm sample and the 280 nm x 400 nm sample at two different excitation wavelength

3.4 Summary

The optical properties of 2D PhC phosphors were examined. Unlike the lateral 1D PhC phosphor, the symmetric 2D PhC phosphor showed no dependence on the polarization direction of the external excitation source. In the asymmetric 2D PhC phosphor, both emission resonance and excitation resonance occurred, resulting in higher enhancement factor.

FDTD and PWE methods were used to examine photonic band structures and absorbance spectra of 2D PhC phosphors. This confirmed the polarization independence property of the symmetric 2D PhC phosphor and the fact that both emission resonance and excitation resonance could occur in the asymmetric 2D PhC phosphor.

2D PhC samples were fabricated with the same process steps as the 1D lateral PhC phosphor, except for an additional exposure on 90°-rotated samples in LHL process.

PL excitation experiments were performed to investigate enhancement factors of 2D PhC phosphors. The symmetric 2D PhC phosphor exhibit nearly the same enhancement factor of ~6 regardless of the polarization direction of excitation source, which is a unique property distinguished from the lateral 1D PhC phosphor. The asymmetric 2D PhC phosphor was improved in fluorescence intensity by ~12 times compared with the reference phosphor due to the fact that both emission resonance and excitation resonance occurred. I expect that the unique properties of these 2D PhC phosphors will be of great help for white LEDs and other applications where efficient white light is required.

References

[1] J. Lee, K. Min, Y. Park, K.-S. Cho, and H. Jeon, "Photonic Crystal Phosphors Integrated on Blue LED Chip for Efficient White Light Generation," Advanced Materials, DOI: 10.1002/adma.201703506 (2017).

[2] K.-M. Ho, C. T. Chan, and C. M. Soukoulis, "Existence of a photonic hap in periodic dielectric structures," Phys. Rev. Lett. 65, 3152 (1990).

[3] R. D. Meade, A. M. Rappe, K. D. Brommer, J. D. Joannopoulos, and O. L. Alerhand, "Accurate theoretical analysis of photonic band-gap materials," Phys. Rev. B. **48**, 8434 (1993).

[4] M. Imada, A. Chutinan, S. Noda, and M. Mochizuki, "Multidirectionally distributed feedback photonic crystal lasers," Phys. Rev. B. **65**, 195306 (2002).

[5] K. Sakai, E. Miyai, T. Sakaguchi, D. Ohnishi, T. Okano, and S. Noda, "Lasing Band-Edge Identification for a Surface-Emitting Photonic Crystal Laser," IEEE J. Sel. Areas Commun. **23**, 1335 (2005).

[6] P. Yeh, *Optical Waves in Layered Media* (Wiley 1988).

[7] K. S. Yee, "Numerical solution of initial boundary value problems involving Maxwell's equations in isotropic media," IEEE Trans. Antennas Propag. **14**, 302 (1996).

[8] W. Hinsberg, F. A. Houle, J. Hoffnagle, M. Sanchez, G. Wallraff, M. Morrison and S. Frank, "Deep-ultraviolet interferometric lithography as a tool for assessment of chemically amplified photoresist performance," J. Vac. Sci. Technol. B **16**, 3689 (1998).

[9] D.-H. Kim, C.-O Cho, Y.-G. Roh, H. Jeon, Y. S. Park, J. Cho, J. S. Im, C. Sone,

Y. Park, W. J. Choi and Q-H. Park, “Enhanced light extraction from GaN-based light-emitting diodes with holographically generated two-dimensional photonic crystal patterns,” Appl. Phys. Lett. **87**, 203508 (2005).

[10] J. H. Moon, S.-M. Yang, D. J. Pine, and W.-S. Chang, “Multiple-exposure holographic lithography with phase shift,” Appl. Phys. Lett. **85**, 4184–4186 (2004).

Chapter 4

Conclusion

In this thesis, I have proposed PhC phosphors as a way to generate efficient white light. I successfully demonstrated efficient white light by integrating both red and green PhC phosphors with a blue LED chip.

Firstly, I designed and fabricated batches of the PhC phosphors using red and green CQDs, with their band-edge resonance tuned at the excitation photon wavelength. The excitation resonance improves the interaction between the excitation photons from the blue LED chip and CQDs, resulting in enhanced absorption of excitation photons by CQDs and thus enhanced emission. Subsequently, I performed PL excitation experiments using a tunable excitation source, in which the excitation wavelength was scanned across the intended resonance wavelength to investigate properties of the fabricated PhC phosphors. Red and green PhC phosphors showed improved fluorescence intensity by ~5.5 times and ~3.1 times, respectively, compare with the reference phosphors. Next, white light was generated by stacking the red and green PhC phosphors on a blue LED chip. I observed 8% stronger white light out of 33% less CQD amounts in comparison with the structure-less reference phosphors, thanks to a higher color conversion efficiency enabled by PBE effect.

Next, I examined the optical properties of 2D PhC phosphors. Numerical

simulations showed that the polarization independence property of symmetric 2D PhC phosphors and the fact that both emission resonance and excitation resonance could occur in the asymmetric 2D PhC phosphor. PL excitation experiments were performed to verify the simulation results. The symmetric 2D PhC phosphor exhibited nearly the same enhancement factor of ~6.0 regardless of the polarization direction of excitation source. The asymmetric 2D PhC phosphor exhibited higher enhancement factor (~12) than 1D lateral PhC phosphor or symmetric 2D PhC phosphor due to the fact that both emission resonance and excitation resonance occurred.

These results prove that our PhC phosphor platform is not just a conceptual advancement but also a viable technology enabled by structurally engineering any phosphor materials. I believe that PhC phosphor platform is a paradigm-shifting way of developing next-generation high efficiency phosphors.

국문 초록

오늘날 고효율 백색광원의 구현은 디스플레이 패널의 백라이트, 전장, 일반조명 등의 다양한 활용에 있어서 매우 중요하다. 특히 백색 발광다이오드는 고효율, 친환경, 긴 수명, 작은 크기 등의 고유한 장점들로 인하여 많은 주목을 받아왔다. 백색광을 만드는 가장 일반적인 방법은 청색 발광 다이오드를 하나 또는 그 이상의 파장 변환 형광체와 결합하는 것이다. 따라서 형광체는 백색 발광다이오드의 구현에 있어서 청색 발광다이오드 칩만큼이나 중요하다고 해도 과언이 아니다. 하지만 지금까지의 형광체 연구는 기존 형광체 물질의 특성 향상이나 새로운 형광체의 개발 등 주로 물질개발 측면에 집중해 왔다. 우리 연구팀은 이런 물질 기반의 형광체 연구에 대한 대안으로 구조적인 측면에서의 접근, 즉 광자결정 형광체를 제시하고 시연하였다. 광밴드엣지 모드에서 빛의 군속도는 영에 가깝게 되며 이로 인하여 빛과 물질간의 상호작용이 극대화 된다. 따라서 광자결정에 형광체를 결합하고 광밴드엣지 모드를 여기 광자의 에너지에 맞추어 줌으로써 빛과 형광체의 상호작용을 극대화 시켜 색 변환 효율을 향상 시킬 수 있었다.

본 학위 논문에서는 청색 발광다이오드 위에 광자결정 형광체를 여러 장 쌓아서 효율적인 백색광을 구현하는 방법을 제안하였다. 적색 및 녹색 콜로이드 양자점을 사용하여 구조의 광밴드엣지 모드가 여기 광자의 파장에 맞추어진 광자결정 형광체를 설계 제작하였다. 제작된 광자결정 형광체를 청색 발광다이오드와 결합시키면 광밴드엣지 효과에 의하여 청색 발광다이오드로부터 방출된 광자와 콜로이드 양자점의 상호작용이 증가되고 더 많은 광자가 콜로이드 양자점으로 흡수되어 콜로이드 양자점의 발광 세기 또한 증가하게 된다. 적색 및 녹색 광자결정 형광체를 청색 발광다이오드 위에 여러 장 쌓아서

백색광을 구현하였다. 이렇게 구현된 백색광은 광밴드엣지 효과에 의한 광변환 효율 증가로 인하여 아무 구조가 없는 비교 형광체로 만들어진 백색광 보다 33%나 적은 양의 콜로이드 양자점을 사용했음에도 불구하고 8% 향상된 방출 세기를 나타내었다.

또한 2차원 광자결정 형광체의 광학적 특성을 연구하였다. 대칭 2차원 광자결정 형광체는 여기 광원의 편광 방향과 상관없이 약 6배의 광 세기 증가를 보였으며, 비대칭 광자결정 형광체에서는 여기 공명과 발출 공명이 모두 일어남으로 인하여 다른 광자결정 형광체 구조들 보다 더 큰 12배 정도의 광 세기 증가를 보였다.

이상의 결과들을 토대로 구조 설계 및 제작 공정 등에서 더 최적화가 진행된다면 형광체, 백색 발광다이오드 및 효율적인 백색광이 필요한 다양한 분야에서 본 연구는 큰 도움이 될 것이라 예상한다.

핵심어: 백색광, 콜로이드 양자점, 광자결정 형광체, 광밴드엣지,

학번: 2013-30118